Renewable Energy 112 (2017) 166–186

Contents lists available at ScienceDirect

Renewable Energy

journal homepage: www.elsevier.com/locate/renene

A coupled optical-thermal-electrical model to predict the performance of hybrid PV/T-CCPC roof-top systems

W. Li [a], M.C. Paul [a, *], M. Rolley [b], T. Sweet [b], M. Gao [b], H. Baig [c], E.F. Fernandez [d], T.K. Mallick [c], A. Montecucco [a], J. Siviter [a], A.R. Knox [a], G. Han [e], D.H. Gregory [e], F. Azough [f], R. Freer [f]

[a] School of Engineering, University of Glasgow, Glasgow, G12 8QQ, UK
[b] School of Engineering, Cardiff University, Cardiff, CF24 3AA, UK
[c] Environment and Sustainability Institute, University of Exeter, Penryn, TR10 9FE, UK
[d] Centre for Advanced Studies in Energy and Environment, University of Jaen, Jaen, 23071, Spain
[e] WestCHEM, School of Chemistry, University of Glasgow, Glasgow, G12 8QQ, UK
[f] School of Materials, University of Manchester, Manchester, M13 9PL, UK

ARTICLE INFO

Article history:
Received 21 November 2016
Received in revised form
24 April 2017
Accepted 2 May 2017
Available online 3 May 2017

Keywords:
Solar energy
Crossed compound parabolic concentrator
Photovoltaic cell
Hybrid solar collector
Outdoor condition
Electrical model

ABSTRACT

A crossed compound parabolic concentrator (CCPC) is applied into a photovoltaic/thermal (PV/T) hybrid solar collector, i.e. concentrating PV/T (CPV/T) collector, to develop new hybrid roof-top CPV/T systems. However, to optimise the system configuration and operational parameters as well as to predict their performances, a coupled optical, thermal and electrical model is essential. We establish this model by integrating a number of submodels sourced from literature as well as from our recent work on incidence-dependent optical efficiency, six-parameter electrical model and scaling law for outdoor conditions. With the model, electrical performance and cell temperature are predicted on specific days for the roof-top systems installed in Glasgow, Penryn and Jaen. Results obtained by the proposed model reasonably agree with monitored data and it is also clarified that the systems operate under off-optimal operating condition. Long-term electric performance of the CPV/T systems is estimated as well. In addition, effects of transient terms in heat transfer and diffuse solar irradiance on electric energy are identified and discussed.

1. Introduction

Flat-plate photovoltaic/thermal (PV/T) hybrid solar collectors, first-time proposed in 1978 [1] and later tested by Ref. [2], have been developed over the years for efficient solar energy utilization – excellent reviews of this subject were provided in Refs. [3,4]. In Ref. [5], a Solarex MSX60 polycrystalline flat-plat PV module was integrated with a heat collecting plate to form a PV/T module and both the electrical and thermal performances of the module were tested. The module showing its primary-energy saving efficiency exceeds 0.6 in comparison with a pure solar thermal collector. Hourly and monthly electrical and thermal performances of a PV/T array were predicted under Cyprus [6] and Greece [7] climate conditions by using TRNSYS software. Various design methods were discussed in Ref. [8] to improve the electrical and thermal performances of a flat-plat PV/T hybrid air collector. Effects of water flow rate and packing factor on the energy performance of a façade-integrated PV/T system were predicted and clarified by using a lumped thermal model [9].

The overall performance of a PV/T collector with and without glass cover was also analysed in Ref. [10] and a PV/T collector with glass cover having a better performance was identified. A thermal model of a UK domestic PV/T system was established in Ref. [11], and the packing factor of solar cells and water flow rate was optimized. A full unsteady, 3D numerical thermal model was developed in Ref. [12] to investigate the hourly and monthly electrical and thermal performances of a flat-plat PV/T system, and it was shown that the use of time-averaged climate can lead to an overestimation of the thermal performance.

To improve overall performance of flat-plate PV/T collectors, a PV/T roof-top system with crossed compound parabolic

* Corresponding author.
E-mail address: Manosh.Paul@glasgow.ac.uk (M.C. Paul).

http://dx.doi.org/10.1016/j.renene.2017.05.012

Nomenclature

a_1, a_2, a_3 coefficients in Eq. (1) respectively related to glass reflectance, absorptance of PV cells and absorber, PV cell parking/active area
A_c collecting area of CPV/T module
A_{cell} area of all the cells in a CPV/T module
A_h cross-sectional area of flow channels in a heat exchanger, m^2
b gap/spacing between two plates in a finned heat exchanger, m
B^j control function of mass flow rate between two segments of water body in a tank in Eq. (12)
c_1, c_2 empirical constants in Eq. (A2)
C specific heat capacity of a part of CPV/T module, J/(kg K)
C_{fj} water specific heat capacity in the j^{th} segment of water body in a storage tank, $j = 1, 2\ldots, N_t$, J/(kg K)
CR concentration ratio of a CCPC module
d ratio of the diffuse irradiance over the global irradiance on a CPV/T module
E_g band-gap energy of PV cell, eV
E_{PV} instant electrical power generated by PV cells per unit collecting area, W/m^2
g gravitational acceleration, $g = 9.81$ m/s^2
h_{bf} forced convection heat transfer coefficients on the wall of a heat exchanger next to the back cover, W/(m^2 K)
h_{con} free convection heat transfer in the cavity of between the glass cover and the PV cells in a flat PV/T module or in a CCPC cavity, W/(m^2 K)
h_{ga} heat transfer coefficient to account for the radiative heat losses of the top glass cover to the sky plus the wind convection heat transfer coefficient, W/(m^2 K)
h_{pb} radiative heat transfer coefficient of the absorber plate to the back cover, W/(m^2 K)
h_{pg} radiative heat transfer coefficient plus natural convection heat transfer coefficient of the absorber to the glass cover, W/(m^2 K)
h_{pf} forced convection heat transfer coefficients on the wall of a heat exchanger next to the absorber, W/(m^2 K)
h_{sg} radiative heat transfer coefficient plus natural convection heat transfer coefficient of the PV cells to the glass cover, W/(m^2 K)
h_t total heat transfer coefficient between the tank wall and the outside air, W/ K
h_{wind} convection heat transfer coefficient due to wind, W/(m^2 K)
H fin height, m
I current of PV cells/modules, A
I_d diode reversal saturation current, A
I_{ph} photocurrent of PV cells/modules, A
k air/water thermal conductivity, W/(m K)
k_{fin} fin thermal conductivity
L length of flow channels/fins in a heat exchanger, m
m optical gain coefficient of a CCPC module
$\dot{m}_f$ water mass flow rate through a heat exchanger, kg/s
$\dot{m}_{sj}$ mass flow rate between two segments of water body in a tank in Eq. (12), kg/s
M mass of a part of CPV/T module, kg/m^2
n diode quality factor of PV cells/modules
n_1, n_2 empirical powers in Eq. (A2)
N_t total number of segments of water body in a storage tank, $N_t = 10$
Nu Nusselt number of natural convection heat transfer coefficient, $\mathrm{Nu} = h_{con}b/k$
Nu_b Nusselt number of fin channels, $\mathrm{Nu}_b = h_{fin}b/k$, h_{fin} will be either h_{pf} or h_{bf} in Eq. (1) or (1a)
Nu_i ideal Nusselt number of fin channels, defined in Eq. (A4)
Pr fluid Prandtl number, $\mathrm{Pr} = \nu/\tau$
q electron charge, $1.60217646 \times 10^{-19}$C
Ra Rayleigh number of the air between the plates, $\mathrm{Ra} = g\beta'(T_{hot} - T_{cold})b^3/\nu\tau$
Re_b Reynolds number, $\mathrm{Re}_b = Ub/\nu$
Re_b^* Reynolds number of fin channels, $\mathrm{Re}_b^* = \mathrm{Re}_b(b/L)$
R_g reflectance of top glass cover
R_s lumped series resistance of PV cells/modules, Ohm
R_{sh} shunt resistance of PV cells/modules, Ohm
S solar irradiance, W/m^2
t time, s
T Temperature, °C
T_a ambient temperature, °C
T_{cold} the lowest temperature of two plates, K
T_{fi} water temperature at the inlet of the first heat exchanger of CPV/T module, °C
T_{fij} water temperature at the inlet of the first heat exchanger of CPV/T module in the j^{th} month a year, °C
T_{fo} water temperature at the outlet of the last heat exchanger of CPV/T module, °C
T_{fout} temperature of water at the outlet of the last heat exchanger of a CPV/T module, °C
T_{hot} the highest temperature of two plates, K
T_j water temperature in the j^{th} segment of water body in a storage tank, $j = 1, 2\ldots, N_t$
T_{sky} Temperature of the sky, °C
U mean fluid velocity in fin channels, m/s
v_{wind} wind speed, m/s
V output voltage of PV cells/modules, V
V_{fi} water volume in the j^{th} segment of water body in a storage tank, $j = 1, 2\ldots, N_t$, m^3

Greek symbols

α absorption coefficient of top glass cover or PV cell or absorber
β tilted angle of a CPV/T module, °
β' volumetric coefficient of expansion of air
γ experimental incidence angle modifier coefficient
δ thickness of fin, mm
ε emissivity of a part of CPV/T module
η_{opt} optical efficiency of a CCPC module
θ solar beam incidence angle on a CPV/T module, °
θ_{eff} effective incidence angle of diffuse irradiance, °
κ Boltzmann constant, $1.38065031 \times 10^{-23}$J/K
μ temperature coefficient of short circuit current, A/K
ν kinematic viscosity of fluid, m^2/s
ρ_{fj} water density in the j^{th} segment of water body in a storage tank, $j = 1, 2\ldots, N_t$, kg/m^3
σ Stefan-Boltzman constant, 5.670367×10^{-8} kg s^{-3} K^{-4}
τ thermal diffusivity of air, m^2/s

Subscripts

0	Standard test condition in PV cell/module indoor experiment
b	back cover
f	water in heat exchanger
g	top glass cover
p	absorber
s	solar/PV cell
j	index of segments of water body in a tank or month a year

Abbreviation

3D	three dimensional
CCPC	crossed compound parabolic concentrator
CFD	computational fluid dynamics
CPC	compound parabolic concentrator
CPV/T	concentrating PV/T
IAM	incidence angle modifier
MPP	maximum power point
MPPT	maximum power point tracer
PV/T	photovoltaic/thermal

concentrator (CCPC) was proposed in Ref. [13]. The system mainly consists of a series of CCPCs, flat-plate PV cells and finned heat exchanger as well as a glazed case. The CCPCs are glued on the top of the heat exchanger and the PV cells are installed in the CCPC aperture each.

Recently, a computational fluid dynamics (CFD) method has been applied to characterise the optical and thermal performance of a CCPC with PV cell [14]. However, this method was incapable of analysing a concentrating PV/T (CPV/T) hybrid roof-top system from a system point of view.

In this article, we aim to develop a coupled lumped optical, thermal and electrical model to examine the electrical performance of the CPV/T roof-top systems installed in three different geographical locations which operate under variable outdoor climate conditions. The model should be sufficiently robust to allow us to clarify their performance very rapidly, thus aiding to optimise the major design variables and water flow rate through heat exchangers for the systems installed in different places.

Existing models for predicting the thermal performance of solar thermal collectors with compound parabolic concentrator (CPC), i.e. trough, were proposed in Ref. [15]. In the models, the optical efficiency was assumed constant and expressed analytically in terms of the average number of reflections and mirror reflectance of the CPC. The thermal model was for the cylindrical receiver tube installed in a trough. These optical and thermal models were applied to a solar water [16] and air [17] heater with CPC to predict the heater thermal performance. Similarly, these models were used to characterise the thermal performance of a solar air heater designed in Ref. [18].

In Ref. [19], CPC, PV cells and air heat exchanger were integrated together to form a PV/T solar collector. Then, thermal and CPC optical models like those in Refs. [15–18] and a PV cell electrical model were utilized to estimate the collector thermal and electrical performances. Note that the PV cell electrical model was just a general linear correlation of PV cell efficiency with cell temperature proposed by Florschuetz [19].

A double-pass PV/T solar air collector with CPC was proposed in Ref. [20]. The double-pass means the air enters the CPC from its end, and then goes into the finned heat exchanger underneath the PV cells with a 'U' turn, and finally the heated air flows out of the exchanger. The CPC optical and PV cell electrical models were the same as those used in Ref. [19], but the thermal models for the air flow in the CPC and in the finned heat exchanger were newly developed.

A numerical study on the optical and electrical as well as thermal performance of PV/T air collector with CPC of concentration ratio (CR) = 2 was conducted under various ducted heat exchanger lengths and air flow rates at 800 W/m^2 irradiance in Ref. [21]. The optical, thermal and thermal models were taken from Refs. [15–20]. A very similar work can be found in Ref. [22] as well.

A preliminary analytical investigation was carried out on a PV/T solar collector with CPC in Ref. [23]. Water was used as a working fluid through a U-type pipe heat exchanger. The optical, thermal and electrical models were identical to those in Refs. [15–20], too. The PV/T performance was estimated at various CRs and PV cell areas under variable solar irradiances and three water mass flow rates.

In Ref. [24], a flat-plate PV system with V-trough was built and measured under outdoor conditions and the cooling effect on the PV system electrical performance was explored. The optical model in Ref. [25] and the thermal model for the heat exchanger with cooling water in Ref. [26], the electrical model for PV modules in Ref. [27] and the scaling law for outdoor conditions in Refs. [26–29] were combined together to predict the optical, cell temperature and electrical power of the system. It should be pointed out that the solar beam incidence was involved in the optical model but the diffuse component in the solar radiation was neglected.

In this article, a coupled lumped optical, thermal and electrical model is developed by involving variable optical efficiency with new natural heat transfer coefficient for CCPCs and finned heat exchangers. At first, a set of mathematical equations are reformulated based on those in Refs. [19,30] by adapting new convection heat transfer coefficients for water flow in the heat exchanger in a PV/T collector and for the air flow in the cavity of CCPC. Then, an optical model with a variable optical efficiency is developed in terms of incidence. Additionally, the optical and thermal models are incorporated with an electrical model for PV electrical module with CCPC in Ref. [31] and the scaling law in Ref. [32]. Finally, the models are applied to estimate the electrical performance of the PV/T roof-top system based on hourly monitored solar irradiance, ambient temperature, wind speed and water at the inlet of the first heat exchanger in a day in three different places.

Further, the proposed model itself is innovative because it incorporates the optical efficiency of a CCPC which is correlated with the incidence of solar radiation beam through the optical model. A new scaling law for the electrical model of the PV modules with CCPCs has been developed in-house and utilized here to operate under outdoor conditions. Additionally, convection heat transfer coefficients depending on both CR and inclination angle of CCPCs are adapted in finned heat exchangers to account the low Reynolds number flow effects. Furthermore, diffuse solar radiation component is also included in the model. To the best of the authors' knowledge, no existing model in the literature provides all these innovative features which are vital for the characterisation of hybrid PV/T-CCPC roof-top systems.

2. Roof-top systems

Photographs of the roof-top PV/T systems installed in Glasgow, Penryn and Jaen are shown in Fig. 1 (a)-(c) respectively. The system has an insulation case with a top glass cover and PV/T modules inside. Under each PV/T module, a finned heat exchanger, which has the same structure and dimensions to the finned heat exchanger described in Ref. [33], is installed. Water stored in the tank (690 × 515 × 520 mm) is driven by a pump, which flows from one heat exchanger to next one in a series to cool down the PV cells

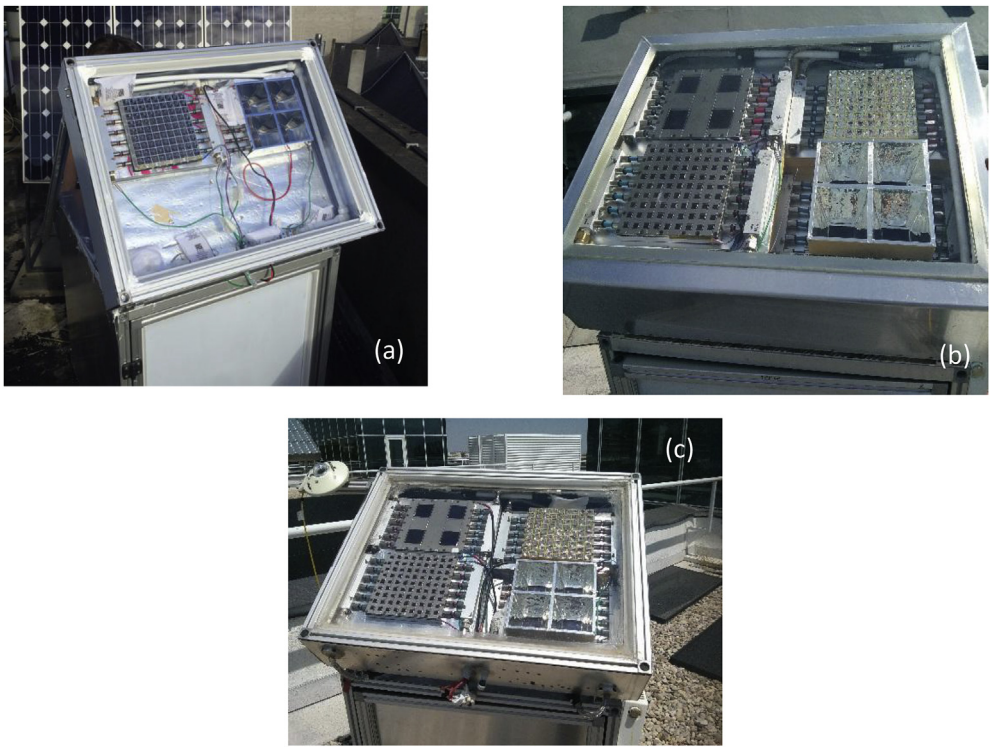

Fig. 1. Three roof-top systems designed for SUNTRAP project, (a) two 2 × 2 and 9 × 9CCPC modules installed at the University of Glasgow, Scotland, (b) 9 × 9flat, 9 × 9CCPC, 2 × 2flat and 2 × 2CCPC modules installed at the University of Exeter, Penryn, England, (c) 9 × 9flat, 9 × 9CCPC, 2 × 2flat and 2 × 2CCPC modules installed at the University of Jaen, Spain.

glued outside the exchangers and finally returns to the storage tank.

As seen in Fig. 1(a), the system consists of 2 × 2 and 9 × 9 CCPC modules with 2 × 2 (cells in 50.5 × 50.5 mm^2 size) and 9 × 9 (cells in 10 × 10 mm^2 size) PV cells underneath. The modules have a collecting area of 0.213 × 0.213 m^2. The acceptance angle of these CCPCs is 20°. The finned heat exchangers are made of aluminium with 205 W/(m^2 K) thermal conductivity and have 46 fins each with 10 mm height, 1 mm spacing and 3 mm thickness. Note that the gap between the PV cells and the top glass cover is 37.5 mm in the PV/T modules. This system was installed on a building roof at the University of Glasgow campus in Scotland.

The system shown in Fig. 1(b), installed on a building top at the University of Exeter, Penryn, England, is composed of two 2 × 2 and 9 × 9 flat PV modules and two 2 × 2 and 9 × 9 CCPC modules. The heat exchangers of 9 × 9 flat, 9 × 9 CCPC, 2 × 2 flat, 2 × 2 CCPC are connected to each other in a series. The same system is installed on a building top at the University of Jaen, Spain, and the three roof-top systems share the same geometrical dimensions and structure.

To illustrate the working situation and testing instruments of the three roof-top systems mentioned above, their block diagrams are presented in Fig. 2, in which Fig. 2(a) represents the block diagram of the roof-top system shown in Fig. 1(a), i.e. a two-stage system, while Fig. 2(b) stands for the block diagram of the roof-top systems in Fig. 1(b) and (c), i.e. a four-stage system. The testing instrumentations for characterizing the electrical and thermal performances of three CPV/T systems are also illustrated in Fig. 2(c). The thermocouples at the heat exchange inlet and out and on the top of the water tank are used to monitor the water temperature. The data logger controls the signal to operate the pumps and the electric circuit load, and also acquires voltage, current, temperature and flow meter frequency. An in-house developed maximum power point tracer (MPPT) was applied to track the maximum power point (MPP) of an I-V curve. Additionally, a pyranometer (CPM11) was installed beside the PV case to monitor the solar irradiance. Even though the tilted angle of the CPV/T system is adjustable manually, it is fixed all the time in three sites mentioned above.

The coordinates and annual average meteorological parameters in Glasgow, Penryn and Jaen are presented in Table 1. The annual average global solar energy in Penryn is around 20% higher than that in Glasgow, while the annual average global solar energy is doubled in Jaen in comparison with that in Glasgow (1094 kWh/m^2).

3. Modelling methods

If the block diagrams in Fig. 2 are looked at carefully, they are essentially composed of two elementary PV/T modules, i.e. a flat PV/T module and a PV/T module with CCPC, as shown in Fig. 3. At first, we establish optical, thermal and electrical models for these elementary PV/T modules, respectively, then combine them together according to the actual components of a roof-top system shown in Fig. 1(a)-(c). Finally, performance of the roof-top system is predicted by using the combined models.

To establish a lumped thermal model, as done in Refs. [9,20], it is assumed that the temperature on the top glass cover, PV cells, absorber, and back cover are uniform, but the temperature in the flow medium in the heat exchangers varies linearly from their inlet to outlet. Accordingly, the optical, thermal and electrical coupled transient energy balance equations for the top glass cover, PV cells, absorber, water and back cover of a PV/T system, as shown Fig. 3, can be written as follows:

$$\begin{cases} M_g C_g \dfrac{dT_g}{dt} = a_1 S + h_{pg}(T_p - T_g) + h_{sg}(T_s - T_g) - h_{ga}(T_g - T_a) \\ M_s C_s \dfrac{dT_s}{dt} = a_2 S \times CR \times \eta_{opt} - h_{sp}(T_s - T_p) - h_{sg}(T_s - T_g) - E_{PV} \\ M_p C_p \dfrac{dT_p}{dt} = a_3 S \times CR \times \eta_{opt} + h_{sp}(T_s - T_p) - h_{pg}(T_p - T_g) - h_{pb}(T_p - T_b) - h_{pf}\left(T_p - T_f\right) \\ M_f C_f \dfrac{dT_f}{dt} = h_{pf}\left(T_p - T_f\right) + h_{bf}\left(T_b - T_f\right) - 2\dot{m}_f C_f \left(T_f - T_{fi}\right)\Big/ A_c \\ M_b C_b \dfrac{dT_b}{dt} = h_{pb}(T_p - T_b) - h_{bf}\left(T_b - T_f\right) - h_b(T_b - T_a) \end{cases} \quad (1)$$

where the mass of the glass cover, PV cell, absorber, water and back cover, M_g, M_s, M_p, M_f and M_b have been scaled by using the collecting area; C_g, C_s, C_p, C_f and C_b are the specific heat of the glass cover, PV cell, absorber, water and back cover, J/(kg K) respectively; T_g, T_s, T_p, T_f and T_b are the unknown mean temperatures of the top glass cover, PV cells, absorber, water and back cover, °C. The water mean temperature is represented by $T_f = 0.5(T_{fi} + T_{fo})$, where T_{fi} is a known temperature of fluid at the inlet of a heat exchanger, and T_{fo} is the unknown temperature of fluid at the outlet of the heat exchanger. S is the solar irradiance, W/m^2; $\dot{m}_f$ is the water flow rate through the exchanger, kg/s, CR is the known concentration ratio of CCPC, η_{opt} is the known optical efficiency which can be obtained experimentally or by CFX multiphysics simulation. E_{PV} is the instant electrical power generated by PV cells per unit collecting area.

The coefficients, a_1, a_2 and a_3, in Eq. (1) are related to the glass reflectance, absorptance of the PV cells and absorber, PV cell parking/active area as follows

$$\begin{cases} a_1 = (1 - R_g)\alpha_g \\ a_2 = (1 - R_g)(1 - \alpha_g)(A_{cell}/A_c)\alpha_s \\ a_3 = (1 - R_g)(1 - \alpha_g)(1 - \alpha_s)(1 - A_{cell}/A_c)\alpha_p \end{cases} \quad (2)$$

where $R_g = 0.04$, $\alpha_g = 0.06$ are the reflectance and absorption coefficient for the glass cover, $\alpha_s = 0.674$, $\alpha_p = 0.674$ are the reflectance and absorption coefficient for PV cells and absorber. The solar beam is reflected by the reflective films, thus the corners between the two CCPCs are dark, thus $a_3 = 0$, A_{cell} is the area of all the cells in a PV module and A_c is the collecting area of PV module.

$$\begin{cases} \eta_{\text{opt}} = -3.0278 \times 10^{-3}\theta + 8.4737 \times 10^{-1}, & 0^o \le \theta \le 20^o \\ \eta_{\text{opt}} = -2.2299 \times 10^{-9}\theta^5 + 7.9722 \times 10^{-7}\theta^4 - 1.1161 \times 10^{-4}\theta^3 & \\ \quad +7.6654 \times 10^{-3}\theta^2 - 2.6159 \times 10^{-1}\theta + 3.7257, & 20^o < \theta < 90^o \end{cases} \quad (4)$$

It should be pointed out that the expression of a_2 used in Refs. [19,30] excludes A_{cell}/A_c. Ignoring this term gives an equivalent of PV cells covering the whole surface of absorber and as a result, the energy balance is not held, because an extra energy $(1 - R_g)(1 - \alpha_g)(1 - A_{cell}/A_c)\alpha_s S \times CR \times \eta_{opt}$ will be generated. This overlooking is corrected here.

3.1. Optical model

For a flat PV module or panel, the optical efficiency η_{opt} shown in Eq. (1) is dependent on the solar beam incidence angle θ [34] and expressed by the following expression

$$\eta_{opt} = \eta_{opt}(0)\left[1 - \gamma\left(\frac{1}{\cos\theta} - 1\right)\right] \quad (3)$$

where $\eta_{opt}(0)$ is the optical efficiency at zero incidence i.e. $\theta = 0°$; coefficient a_2 involves the reflection and absorption of the glass, thus $\eta_{opt}(0) = 1$; γ is an experimental incidence angle modifier (IAM) coefficient, $\gamma = 0.05$ [35].

For the CCPC modules with $CR = 3.6$, the optical efficiency was calculated with CFD code ANSYS CFX® and good agreement was achieved between the prediction and the measurement [14]. In the simulations, the solar radiation governing equations were solved by using Monte Carlo method under an assumption that the medium is grey, homogenous with non-scattering reflection, thus the radiative properties of the medium are independent of the wavelength of sunlight. Solar beam reflection and refraction through the interface between two media is considered to be unpolarized two-component radiation with an equal intensity, and the angle of refraction is determined by using the Snell's law of refraction. The air flow inside the CCPC cavity is considered to be steady-state and laminar, and the Boussinesq model is adopted to estimate the density difference in the momentum equations. Finally, in the solid domains, the heat transfer equation through conduction is solved. The resulted optical efficiency was best fitted with a linear and 5th-order polynomial as follows

The curves are compared with the CFX prediction as shown in Fig. 4.

The solar beam incidence on a PV module in daylight period is calculated by using the method suggested in Ref. [26] based on the geographical location of the site where the PV module is installed and its inclination angle at a series of clock time moments from

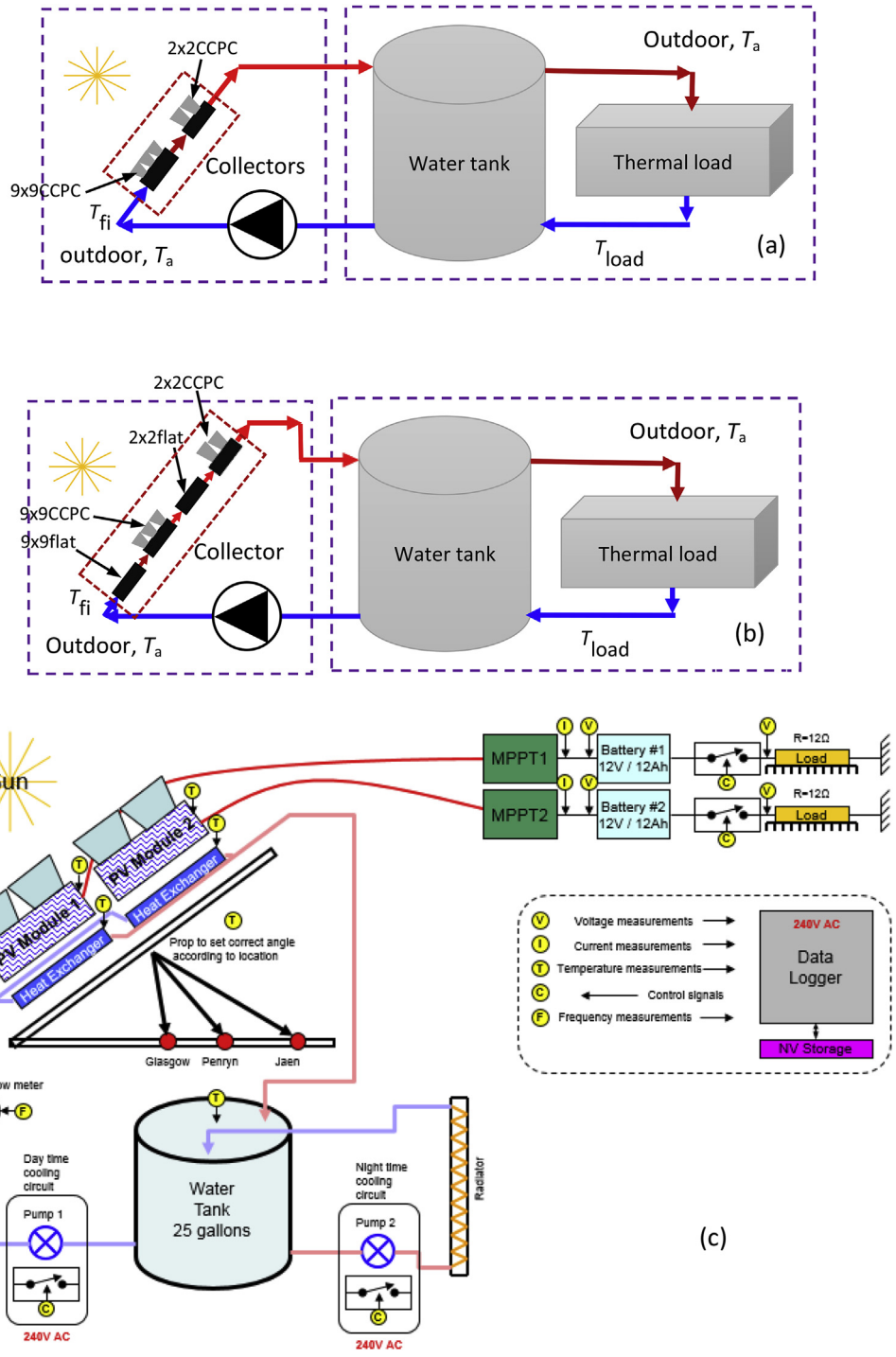

Fig. 2. Block diagrams representing the roof-top systems and testing instruments shown in Fig. 1(a)–(c), (a) two-stage system, (b) four-stage system, (c) testing instruments.

Table 1
Coordinates and annual average meteorological parameters in Glasgow, Penryn and Jaen.

Place	Coordinates	Annual average global solar energy (kWh/m^2)	Annual average diffuse solar energy (kWh/m^2)	Annual ambient temperature (°C)	Annual wind speed (m/s)
Glasgow	55.8642°N 4.2518°W	1094	534	10.20	6.67
Penryn	50.1692°N 5.1071°W	1292	628	11.15	6.30
Jaen	37.7796°N 3.7849°W	2206	621	15.85	1.99

Annual average irradiance (global and diffuse if you have it).

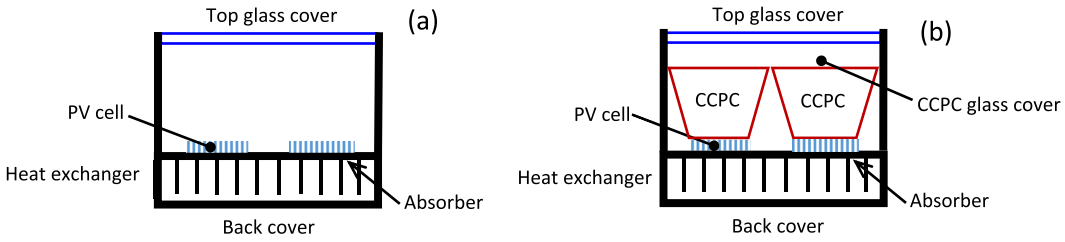

Fig. 3. Two elementary PV/T modules, (a) flat PV/T module, (b) PV/T module with CCPC.

morning to evening.

3.2. Thermal model

In Eq. (1), h_{ga} is the heat transfer coefficient to account for the radiative heat losses of the top glass cover to the sky plus the wind convection heat transfer coefficient. Variables h_{sg} and h_{pg} represent the radiative heat transfer coefficient plus natural convection heat transfer coefficient of the PV cells and absorber to the glass cover, respectively; while h_{pb} is the radiative heat transfer coefficient of the absorber plate to the back cover, $h_{pb} = 0.692$ W/(m^2 K) [19]. These coefficients are written as

$$\begin{cases} h_{ga} = \varepsilon_g \sigma\left(T_g^2 + T_{sky}^2\right)\left(T_g + T_{sky}\right) + h_{wind} \\ T_{sky} = T_a - 20,\ h_{wind} = 5.7 + 3.8 v_{wind} \\ h_{sg} = \dfrac{\sigma\left(T_s^2 + T_g^2\right)(T_s + T_g)}{\dfrac{1}{\varepsilon_s} + \dfrac{1}{\varepsilon_g} - 1} + h_{con} \\ h_{pg} = \dfrac{\sigma\left(T_p^2 + T_g^2\right)(T_p + T_g)}{\dfrac{1}{\varepsilon_p} + \dfrac{1}{\varepsilon_p} - 1} + h_{con} \\ h_{pb} = \dfrac{\sigma\left(T_p^2 + T_b^2\right)(T_p + T_b)}{\dfrac{1}{\varepsilon_p} + \dfrac{1}{\varepsilon_b} - 1} \end{cases} \tag{5}$$

in which the emissivity $\varepsilon_g = \alpha_g$, $\varepsilon_s = \alpha_s$ and $\varepsilon_p = \alpha_p$, σ is the Stefan-Boltzman constant, h_{con} is the free convection heat transfer in the cavity of between the glass cover and PV cells in a flat PV/T module or the CCPC cavity. For the former, the Hollands formula in Ref. [36] is used, which involves module inclination angle; but for the latter, the correlation in Ref. [37] is chosen, in which CR of CCPC and module inclination angle are taken into account. The correlation for the key temperature, T_{sky}, is due to Schott (1985) and is more accurate than the others [38]. The formula of convection heat transfer coefficient due to wind h_{wind}, is developed by McAdams (1954) [39] and is adopted here.

Additionally, in Eq. (1), the forced convection heat transfer coefficients h_{pf} and h_{bf} decide the heat transfer in a heat exchanger. For the channels' fins, an empirical formula given in Ref. [40] is applied to predict the two coefficients according to the known fin geometrical parameters at a low channel Reynolds number in a range 0.1–100. The empirical formulas of the natural and forced heat transfer coefficients are a bit lengthy; one can refer to the appendix for their details.

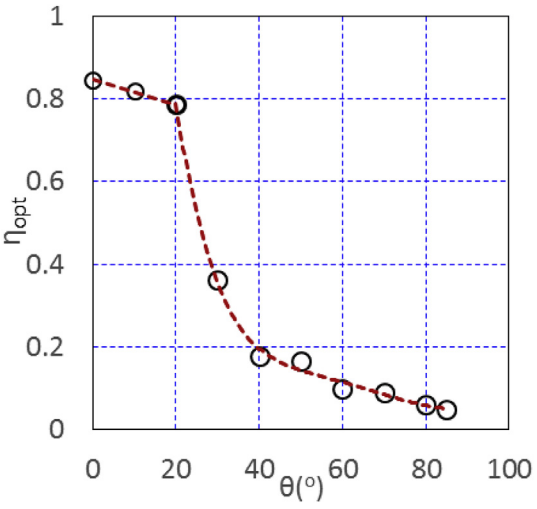

Fig. 4. Comparison of the optical efficiency of a CCPC with $CR = 3.6$ between the CFX prediction and curve fitting, the symbols are for the CFX prediction, the lines for the curve fitting.

3.3. Electrical model

In Eq. (1), E_{PV} represents the electrical power generated by the cells in a PV module per unit collecting area and is calculated by the instant current and voltage of the PV cells by using the following expression under outdoor conditions

$$E_{PV} = V(T_s, S) \times I(T_s, S)/A_c \tag{6}$$

The current-voltage model of PV/T modules have been characterised in our indoor experiment under standard test condition, and they together are illustrated by a scaling law [32]

$$I = I_{ph} - I_d\left\{exp\left[\frac{q(V + R_s I)}{n\kappa T_s}\right] - 1\right\} - \frac{V + R_s I}{R_{sh}} \tag{7}$$

with

$$\begin{cases} R_s = (S_0/S)^{0.7570} R_{s0} \\ I_{ph} = CR^m (S/S_0)^{0.9542}[I_{sh0} + \mu(T_s - T_{s0})] \\ I_d = I_{d0}(T_s/T_{s0})^{-10.6670} \exp\left[\dfrac{1}{\kappa}\left(\dfrac{E_{g0}}{T_{s0}} - \dfrac{E_g}{T_s}\right)\right] \\ E_g/E_{g0} = 1 - 0.0002677(T_s - T_{s0}) \\ R_{sh} = (S_0/S) R_{sh0} \\ n = n_0 \end{cases} \tag{8}$$

where q is the electron charge and κ is the Boltzmann constant,E_g is the band-gap energy of PV cell, $E_{g0} = 1.121$ eV used for diode silicon layer. Note the unit eV is converted to J in the expression of I_d in Eq. (8) with the relationship: 1eV = $1.60217662 \times 10^{-19}$ J. μ is the temperature coefficient of short circuit current,

Table 2
Six parameters extracted for the PV cell/module with CCPC.

Case	$R_{s0}(\Omega)$	$R_{sh0}(\Omega)$	I_{sh0}(A)	$I_{d0}(\mu A)$	n_0	m
Module (2 × 2)	1.8921×10^{-2}	1.2925×10^{3}	2.1404	7.7312×10^{-1}	3.0836	0.6011
Module (9 × 9)	1.1738×10^{-3}	3.0178×10^{3}	3.7717×10^{-1}	3.7721×10^{-1}	10.4431	0.6534

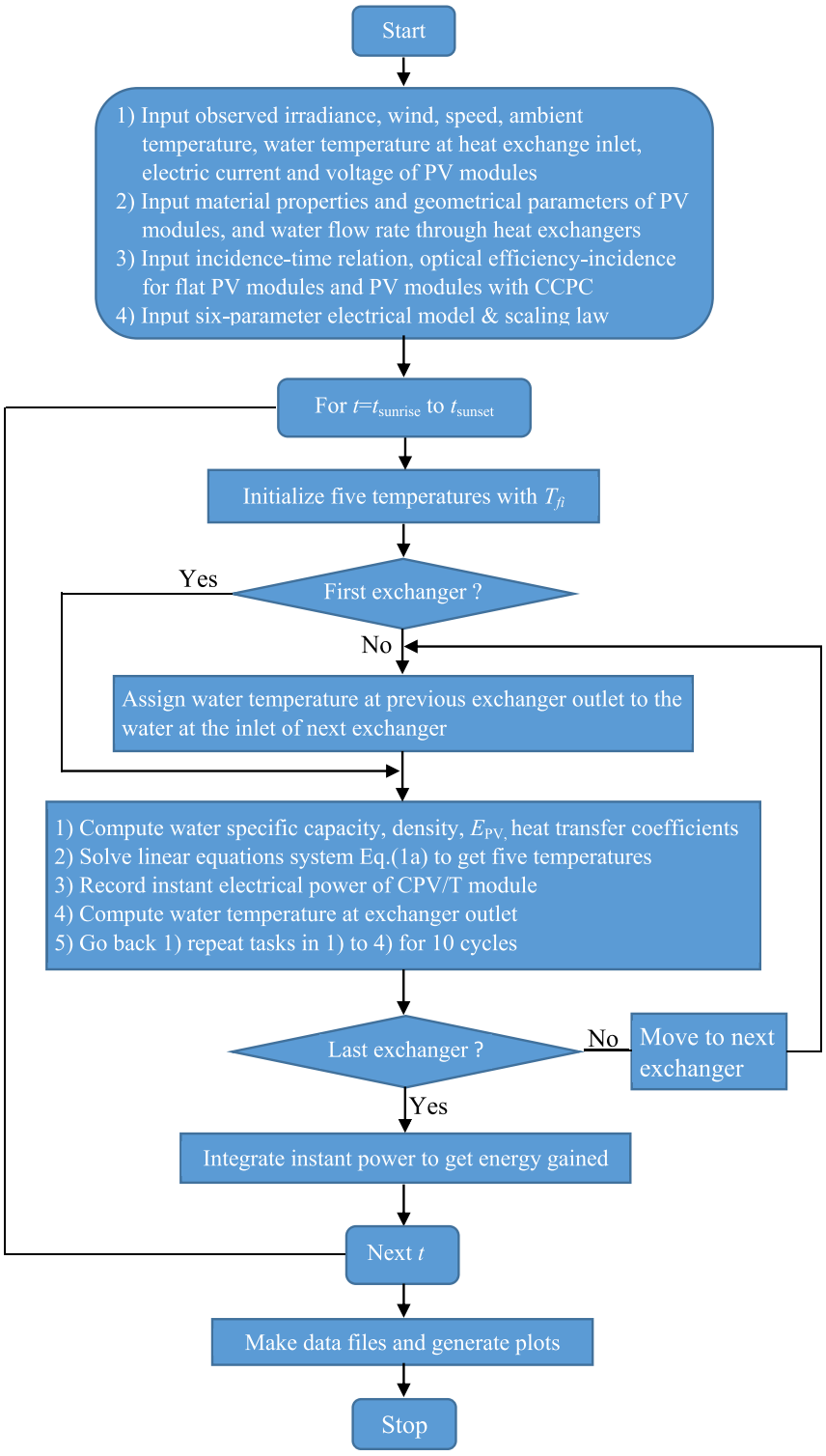

Fig. 5. Flowchart of solution procedure for predicting performance of roof-top systems, $t_{sunrise}$ and t_{sunset} are sunrise and sunset times in a day in a place, t is a time between $t_{sunrise}$ and t_{sunset}.

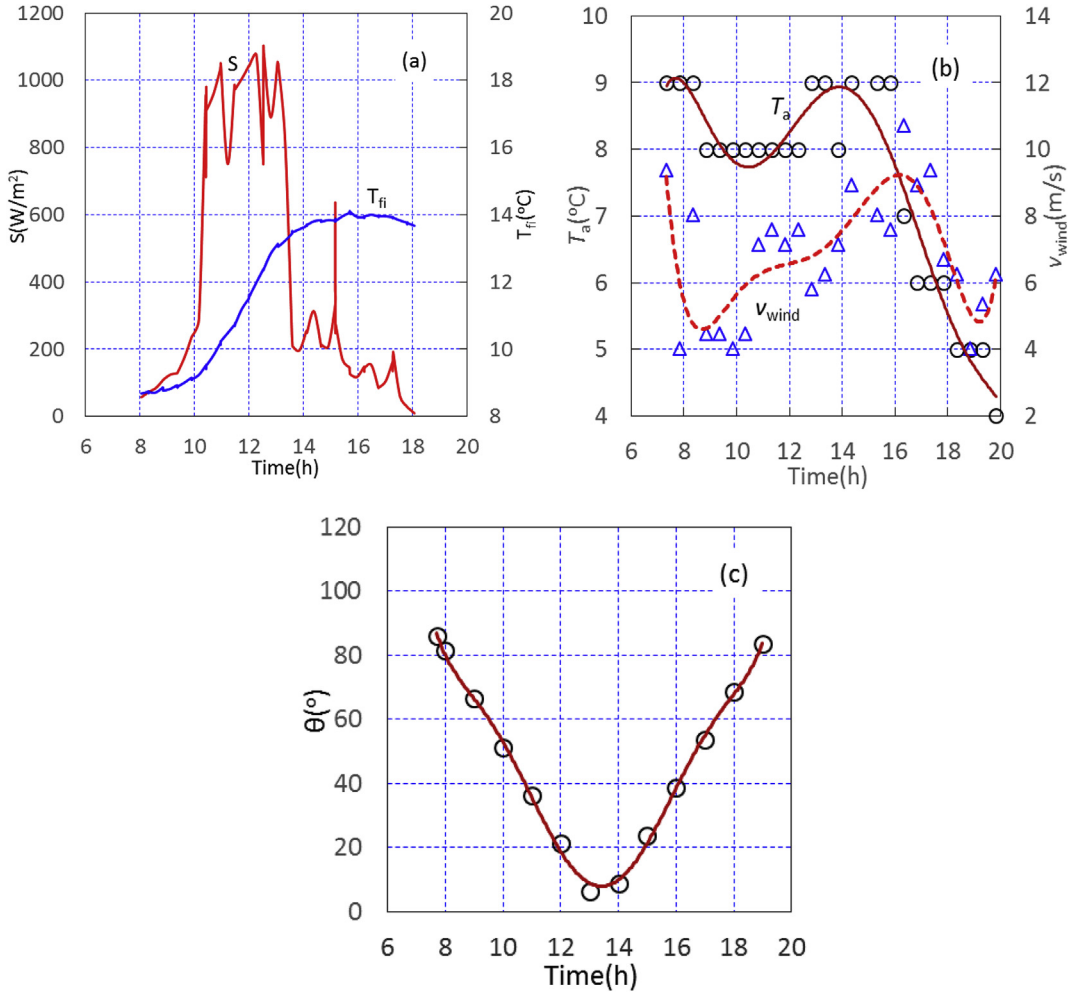

Fig. 6. Monitored solar irradiance on 56° inclined south-faced SUNTRAP roof-top PV/T system, ambient temperature, wind speed and water temperature at the first heat exchanger inlet as well as the incidence estimated are plotted in terms of time on 19 March 2016 in Glasgow, Scotland at $\dot{m}_f = 4.3$ kg/min, (a) irradiance and water temperature, (b) ambient temperature and wind speed, (c) incidence estimated.

$\mu = 3.74 \times 10^{-3} A/K$; $S_0 = 1000$ W/m^2 and $T_{s0} = 298.15$ K [22], the model parameters for the flat and CCPC PV modules are listed in Table 2. Based on Eqs (3), (7) and (8), the electrical power under outdoor conditions can be calculated by means of a series of voltages of a PV module monitored. Note that the irradiance S in the scaling law should be the product of the monitored irradiance and optical efficiency, i.e. $S \times \eta_{opt}$ at every time moment.

3.4. Solution procedure

Note that Eq. (1) is transient, however, the transient effect needs a time-step in second order to get a converged solution for temperatures. As a result, the solution procedure is significantly time-consuming. Therefore, the transient terms in Eq. (1) have been neglected as done in Refs. [19,30]. Eventually, the heat transfer balance equations are rewritten in the following form

$$\begin{cases} (h_{ga}+h_{sg}+h_{pg})T_g - h_{sg}T_s - h_{pg}T_p = a_1 S + h_{ga}T_a \\ -h_{sg}T_g + (h_{sg}+h_{sp})T_s - h_{sp}T_p = a_2 S \times CR \times \eta_{opt} - E_{PV} \\ -h_{pg}T_g + \left(h_{sp}+h_{pg}+h_{pb}+h_{pf}\right)T_p - h_{sp}T_s - h_{pf}T_f - h_{pb}T_b = a_3 S \times CR \times \eta_{opt} \\ -h_{pf}T_p + \left(h_{pf}+h_{bf}+2\dot{m}_f C_f / A_c\right)T_f - h_{bf}T_b = 2\dot{m}_f C_f T_{fi} / A_c \\ -h_{pb}T_p - h_{bf}T_f + \left(h_{pb}+h_{bf}+h_b\right)T_b = h_b T_a \end{cases} \quad (1a)$$

To justify the simplification above, a comparison with the transient model will be made and discussed in Section 4.3.1.

Since the solar irradiance S, ambient T_a, optical efficiency η_{opt} and water temperature at the first heat exchanger inlet T_{fi} in Eq. (1a) as well as wind speed v_{wind} in Eq. (5) are known and even though the transient terms disappear, Eq. (1a) is still time-

dependent because the irradiance, wind speed and ambient temperature are time-dependent and exhibits a quasi-steady behaviour.

Additionally, the heat transfer coefficients in Eq. (1a) depend on unknown temperatures themselves except the heat conductance between the PV cells and the absorber h_{sp} = 150 W/(m^2 °C). Consequently, an iterative algorithm is needed. In doing so, firstly, the initial temperatures are assigned with T_{fi}, then the heat transfer coefficients are calculated from Eqs. (5), and (A1)–(A4) with the initial temperatures. Eq. (1a) is solved in MATLAB with an embedded function-*linsolve* based on these temporary coefficients to secure an updated set of temperatures. Thirdly, a new set of heat transfer coefficients are worked out with these updated temperatures and Eq. (1a) is solved once again with the new set of coefficients to obtain a new set of unknown temperatures. Such a cycle is repeated until the temperature no longer changes and it is shown that ten iterative cycles are adequate. A flowchart for this procedure is shown in Fig. 5.

Further, in the roof-top systems shown in Fig. 1, the heat exchangers are connected in series. At a time instant, the solution process proceeds from the fist PV/T module to another until the last one is achieved by assigning the water temperature at a heat exchange outlet to the water temperature at the next heat exchanger inlet. This procedure is followed to the next time instant until the sunset.

4. Results and discussions

4.1. Daily performance predictions and comparison with outdoor observations

To predict the electrical performance of the roof-top system in Fig. 1, the solar irradiance on the inclined PV/T module top glass cover, ambient temperature, wind speed and water temperature at the first heat exchanger inlet in clear days, namely on 19 March 2016 in Glasgow, Scotland, on 17 September 2015 in Penryn, England and on 11 July 2016 in Jaen, Spain are extracted from the monitored data sets, and are illustrated in Figs. 6–8. The solar irradiance profiles exhibit a significant fluctuation in Glasgow and Penryn, especially in Penryn, mainly because of moving clouds. The incidence variations as a function of time are determined by using the method in Ref. [26].

The predicted electric power, electric energy and cell temperature in the 56° inclined south-faced roof-top PV/T system on 19 March 2016 in Glasgow at $\dot{m}_f$ = 4.3 kg/min flow rate are presented in Fig. 9. Since the solar irradiance is in peak and the incidence is reasonably small during 11:00–13:00, both the predicted and observed electric power in the two PV modules have a high yield, as shown in Fig. 9(a) and (b). The accumulated total electric energy harvest also increases rapidly within that period of time followed by a steady growth, seen in Fig. 9(c). The average error between the prediction and the observation is 13.47 ± 2.22%. Generally, the

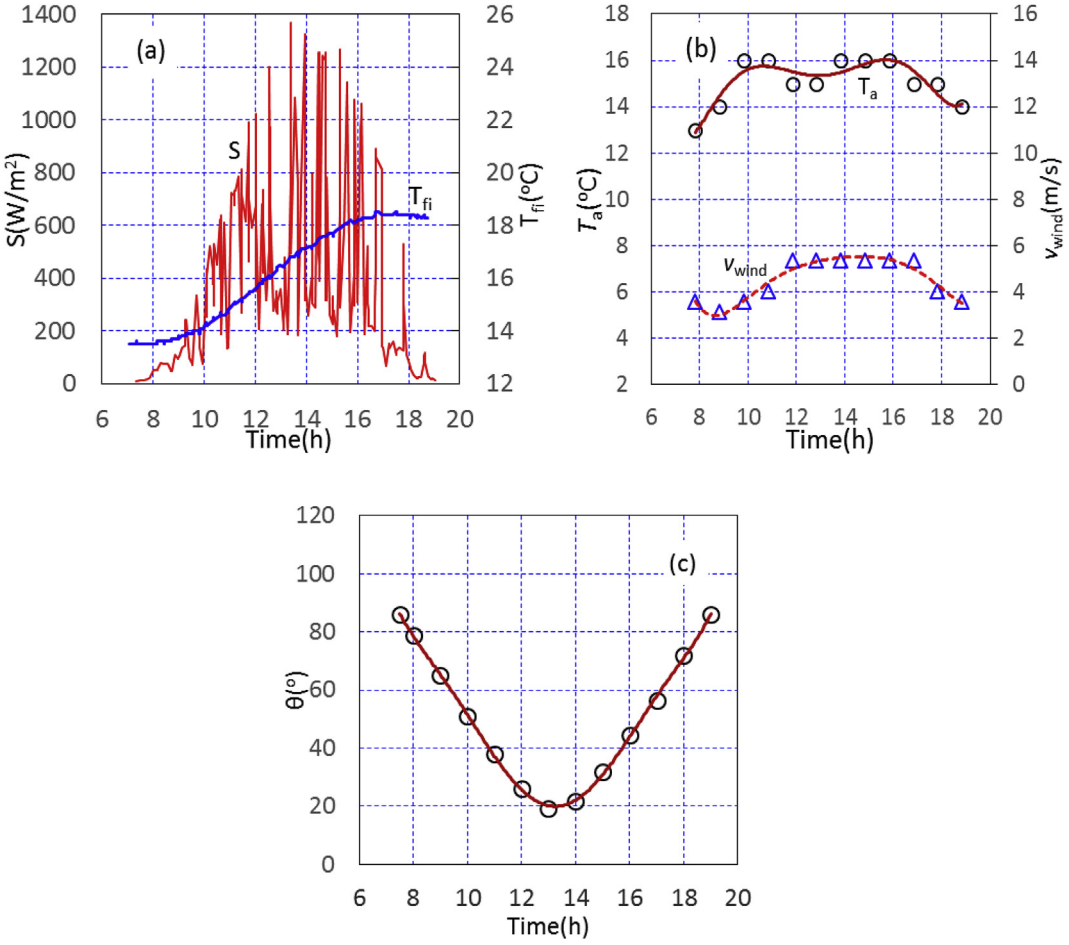

Fig. 7. Monitored solar irradiance on 30° inclined south-faced SUNTRAP roof-top PV/T system, ambient temperature, wind speed and water temperature at the first heat exchanger inlet as well as the incidence estimated are plotted in terms of time on 17 September 2015 in Penryn, England at $\dot{m}_f$ = 2.96 kg/min flow rate, (a) irradiance and water temperature, (b) ambient temperature and wind speed, (c) incidence estimated.

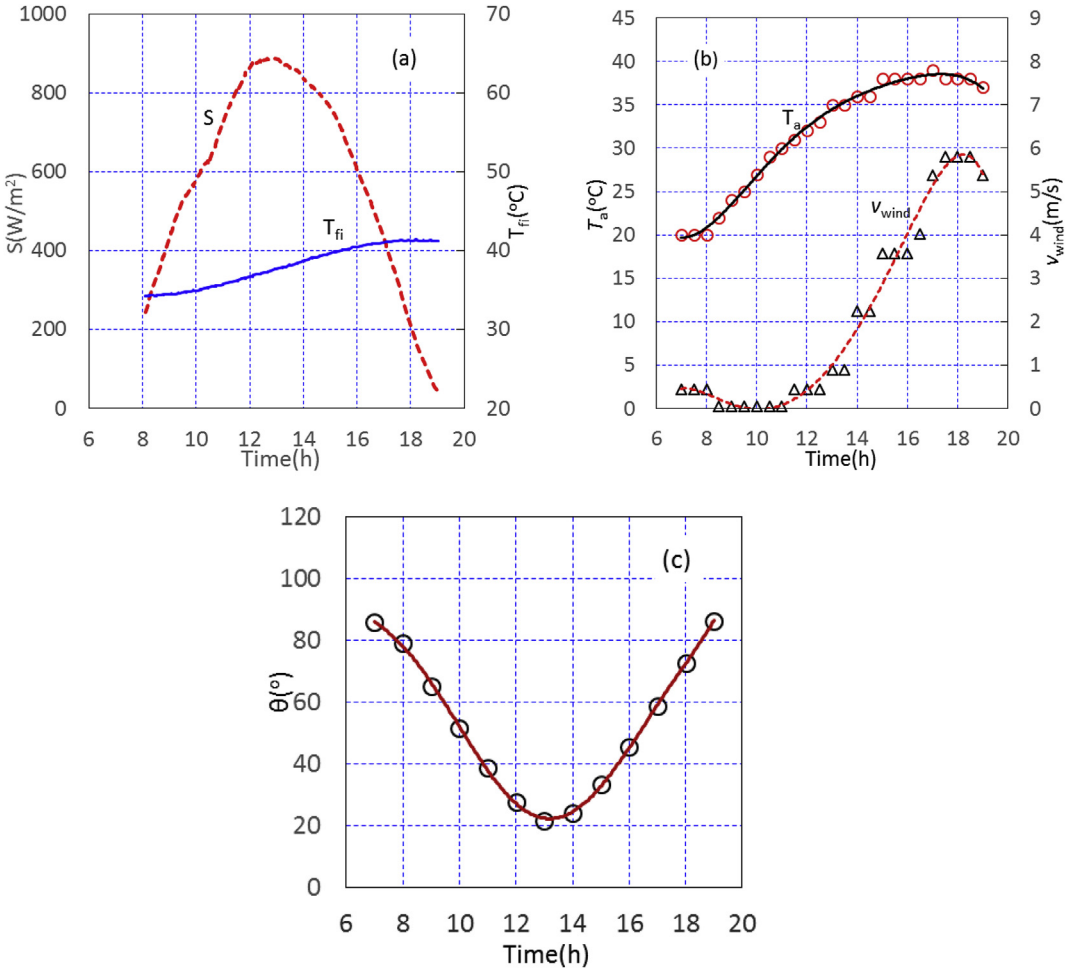

Fig. 8. Monitored solar irradiance on 38° inclined south-faced SUNTRAP roof-top PV/T system, ambient temperature, wind speed and water temperature at the first heat exchanger inlet as well as the incidence estimated are plotted in terms of time on 11 July 2016 in Jaen, Spain at $\dot{m}_f$ = 1.24 kg/min, (a) irradiance and water temperature, (b) ambient temperature and wind speed, (c) incidence estimated.

electric power for the 2 × 2 CCPC PV/T module is predicted better than that of the 9 × 9 module. But the issues causing an over-prediction in power will be further discussed in Section 4.3.

The cell temperatures of the two PV/T modules are also in peak during 11:00–13:00 reaching a maximum of 17 °C for the 2 × 2CCPC PV/T module which is slightly higher than that in the first stage, i.e. the 9 × 9CCPC PV/T module. This is considerably higher than the ambient and water temperature which was respectively 8–9 °C and 10–14 °C. But no comparison with experimental data is made here because the cell temperature was unavailable in our three systems. The reason is that measuring cell temperature is quite difficult since there are a large amount of peripheral elements surrounded the cells in a CPV/T system, and it has to be predicted with an empirical correlation or analytical method commonly [41].

Fig. 10 illustrates the results of the roof-top CPV/T system in Penryn installed at 30° south facing and operated at $\dot{m}_f$ = 2.96 kg/min flow rate. It is shown in Fig. 7 that the solar beam incidence is always larger than 20°, which is beyond the optimal range of incidence [13,14]. Here, the optimal incidence range of a CCPC is defined as the range in which the CCPC optical efficiency is the maximum. For the CCPCs in the paper, their optimal incidence range is 0°-20°. As a result, the two PV/T modules with CCPC just work efficiently at around 14:00 because the maximum irradiance and minimum incidence occur at that time moment. Since the incidence is improper for the two PV/T models with CCPC, their electrical performance is poorer compared with the two flat PV/T modules. Further, the electrical performance of 9 × 9 Flat and 9 × 9 CCPC PV/T models is more ineffective than that of the 2 × 2 Flat and 2 × 2 CCPC PV/T models somehow. Moreover, since the solar irradiance shows significant fluctuation, the cell temperature fluctuates as well. The mean error between the prediction and the observation is 7.17 ± 1.85%.The cell temperature can be as high as 20 °C in comparison with 16 °C maximum ambient temperature and 18.2 °C highest water temperature at the first heat exchanger inlet.

The Jaen system, placed at 38° south facing, shows the two PV/T modules with CCPC start to generate electric power at as late as 10:00 and stop generating electrical power at as early as 15:00 compared with the two flat PV/T modules at 08:00 and 18:00 (Fig. 11) because the electrical power is nearly zero, suggesting the 9 × 9 CCPC and 2 × 2 CCPC PV/T modules are in inefficient operating condition with the incidence always larger than 20°. The electrical power profile of 2 × 2 Flat PV/T module remains to be flat, unlike the profile of 9 × 9 Flat PV/T module. Overall, the electrical performance of the 9 × 9 Flat and 9 × 9 CCPC PV/T modules is better than that of the 2 × 2 Flat and 2 × 2 CCPC modules. This situation seems to be identical to the roof-top system in Glasgow, but the predicted electrical energy is in very good agreement with the observed profile with only a 2.38% variation. The mean error

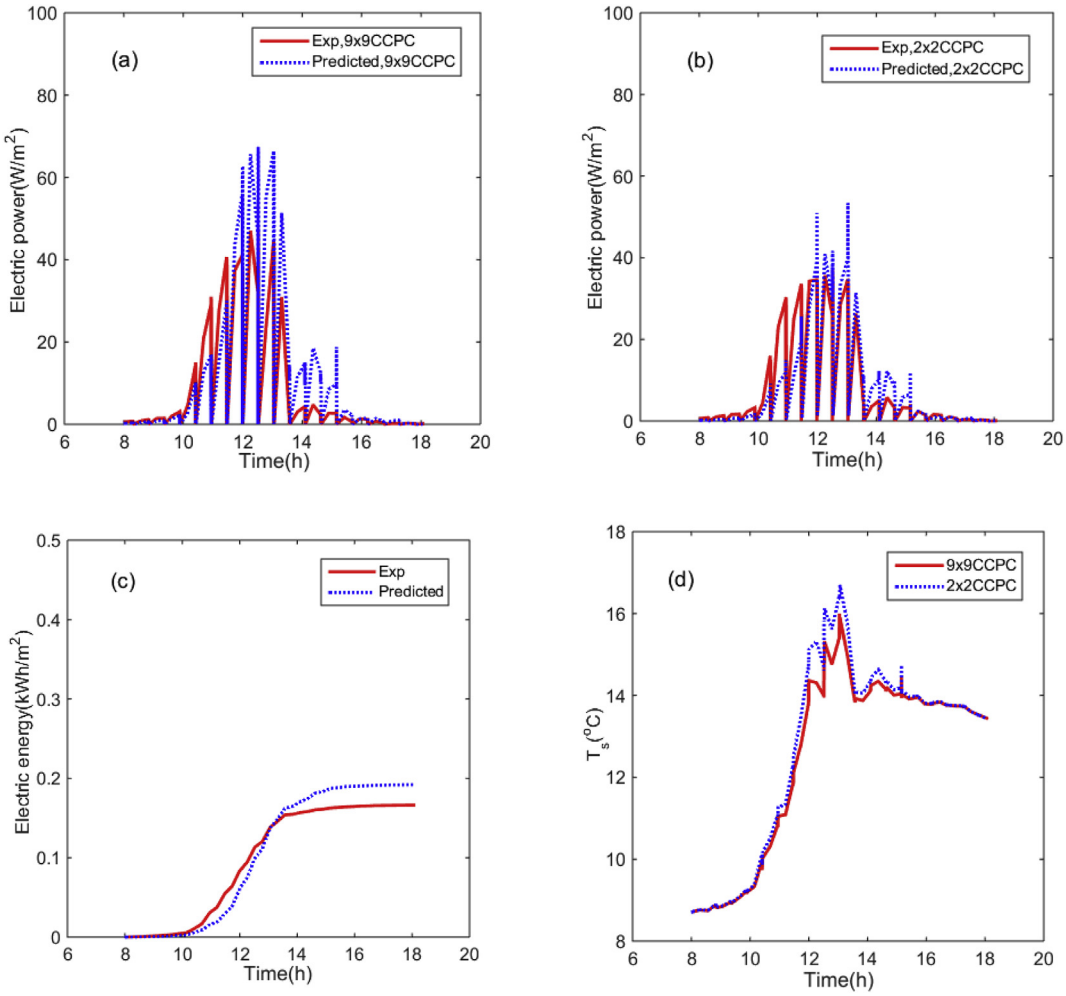

Fig. 9. Predicted and experimental electric power, energy gained and predicted cell temperature in the 56° inclined south-faced SUNTRAP roof-top PV/T system on 19 March 2016 in Glasgow, Scotland at $\dot{m}_f$ = 4.3 kg/min, (a) electric power in 9 × 9CCPC module, (b) electric power in 2 × 2CCPC module, (c) electric energy gained by the system, and (d) cell temperature.

between the prediction and the observation is 2.16 ± 0.67%.

In terms of the temperature variation, the predicted cell temperature can be as high as 41.7 °C, compared with the 38 °C maximum ambient temperature and the 41 °C maximum water temperature at the first heat exchanger inlet. The cell temperature in the two 9 × 9 CCPC and 2 × 2 CCPC PV/T modules is also above the temperature in the two flat PV/T modules only from 11:00 to 16:00, otherwise it is below the temperature in the two flat modules.

Further to note that, in Figs. 9(a) and (b), 10(a)-(d) and 11(a)-(c), although a series of MPPs occur (the peaks in the figures), the zero electric power was measured and predicted even when the irradiance was non zero. This relates to the fact that the instant I-V curves of each module in the CPV/T systems are utilized to estimate the instant electrical power generated in both the observation and prediction operating at a time sequence. In the performance observation of the systems, the electrical circuit voltage was sampled and adjusted automatically and periodically with a certain time step to allow the circuit to experience a few number of states such as open ($I = 0$), short ($V = 0$) circuit and a state in between (I, $V \neq 0$). As a result, a series of I-V curves of each module in the systems are obtained in the time sequence. Thus the electrical power ($I \times V$) is zero at every open ($I = 0$) and short ($V = 0$) circuit point even when the irradiance may not be zero at that time moment.

In the performance predictions, the measured voltage at every time moment together with the corresponding irradiance, cell temperature is used as an input into the scaling law, Eqs. (7) and (8), to determine the electrical current and subsequently the electrical power in order to validate the models proposed in the paper. Likewise, the predicted electrical power is zero at every open and short circuit point even when the irradiance is non zero.

4.2. Annual and monthly predictions

In Section 4.1, short-term electric performance of three CPV/T systems was presented with the proposed coupled lumped optical-thermal-electrical model and a good accuracy has been demonstrated. Here, monthly electric performance of the same four stage CPV/T system when they are installed in Glasgow, Penryn and Jaen, respectively, is predicted to assess their potential electricity production.

Firstly, synthetic climate data in Glasgow, Penryn and Jaen including monthly global radiation, diffuse radiation on a tilted surface, ambient temperature as well as astronomical sunshine duration over 1991–2010 are generated based on the database of software-Meteonorm 7. Then, daily mean irradiance is obtained by dividing the monthly global radiation with the monthly

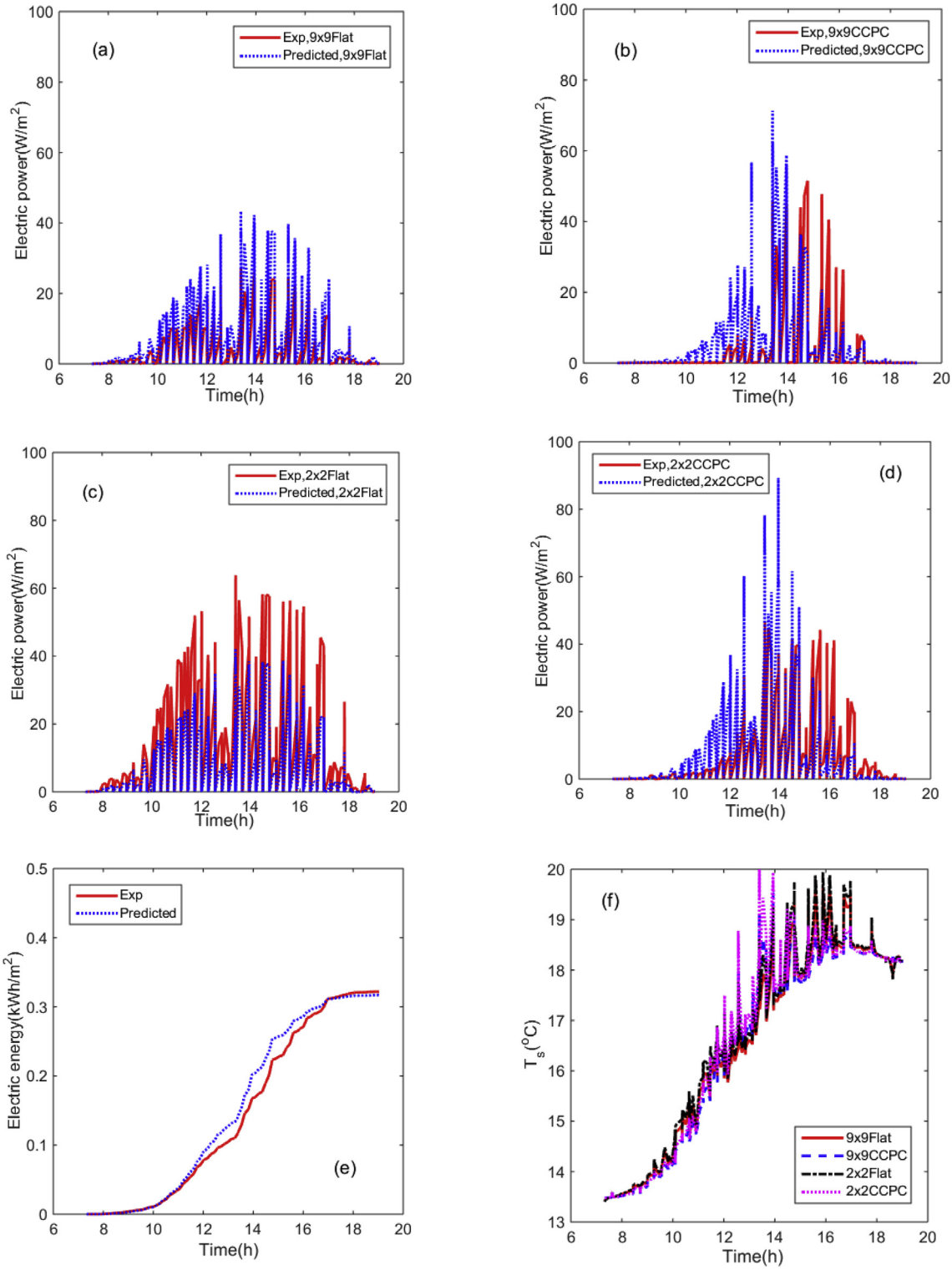

Fig. 10. Predicted and experimental electric power, energy and predicted cell temperature in the 30° inclined south-faced SUNTRAP roof-top PV/T system on 17 September 2015 in Penryn, England at $\dot{m}_f = 2.96$ kg/min, (a) electric power in 9 × 9flat module, (b) electric power in 9 × 9CCPC module, (c) electric power in 2 × 2flat module, (d) electric power in 2 × 2CCPC module, (e) electric energy gained by the system, (f) cell temperature.

astronomical sunshine duration. Thirdly, incidence profiles versus clock time on the average days of month (17th January, 16th in February, 16th in March, 15th in April, 15th in May, 11th in June, 17th in July, 16th in August, 15th in September, 15th in October, 14th in November and 10th in December) specified in Ref. [26] are created by using an in-house MATLAB code based on the method proposed in Ref. [26]. The mean time-weighted incidences are then determined by making use of the incidence profiles.

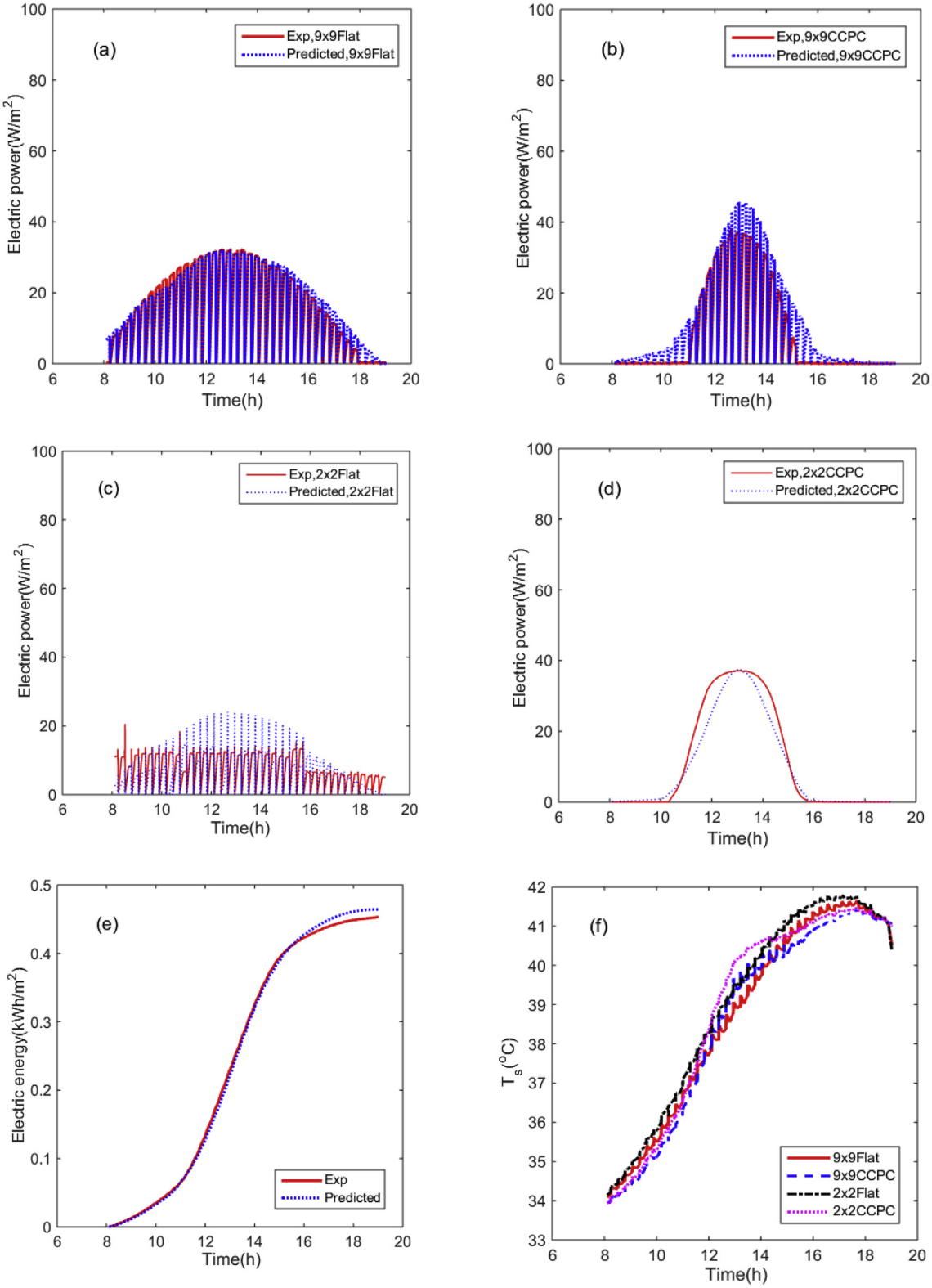

Fig. 11. Predicted and experimental electric power, energy and predicted cell temperature in the 38° inclined south-faced SUNTRAP roof-top PV/T system on 11 July 2016 in Jaen, Spain at $\dot{m}_f = 1.24$ kg/min, (a) electric power in 9 × 9flat module, (b) electric power in 9 × 9CCPC module, (c) electric power in 2 × 2flat module, (d) electric power in 2 × 2CCPC module, (e) electric energy gained by the system, (f) cell temperature.

Table 3
Solar irradiance, ambient temperature and sunshine duration in Glasgow.

Month	Global solar energy (kWh/m^2)	Diffuse solar energy (kWh/m^2)	Ratio of diffuse solar energy	Sunshine duration (h)	Effective clock time(h)		Effective sunshine duration (h)	S (W/m^2)	T_a (°C)	v_{wind}(w/s)	Mean incidence (°)	η_{opt}		Predicted electric energy (kWh/m^2)
					Start	Stop						Flat	CCPC	
Jan	37	15	0.405	248	9	16	217	149.19	4.8	7.73	34.86	0.989	0.256	3.07
Feb	62	23	0.371	280	8	17	252	221.43	5	7.15	37.21	0.987	0.224	5.08
Mar	98	42	0.429	372	8	18	310	263.44	6.8	7.38	38.27	0.986	0.213	7.32
Apr	132	63	0.477	420	7.5	19	345	314.29	9.6	6.97	50.66	0.971	0.142	8.49
May	150	71	0.473	465	7.5	19	356	322.58	12.6	6.71	48.20	0.975	0.150	9.18
Jun	125	76	0.608	480	7.5	19	345	260.42	15.1	6.71	50.04	0.972	0.144	7.02
Jul	131	73	0.557	496	7.5	19	356	264.11	16.4	6.04	49.22	0.973	0.147	7.41
Aug	114	68	0.596	434	7.5	19	356	262.67	16.1	5.81	46.20	0.978	0.158	7.56
Sep	100	42	0.477	360	7.5	19	345	277.78	13.6	6.26	43.47	0.981	0.172	7.97
Oct	65	31	0.477	341	8	18	310	190.62	10.3	6.39	39.50	0.985	0.201	5.13
Nov	49	18	0.367	270	8	16	240	181.48	7.7	6.71	36.74	0.988	0.230	3.98
Dec	31	12	0.387	248	9	15	186	125.00	4.4	6.17	33.52	0.990	0.279	2.27
Year	1094	534	0.488	4414	N/A		3618	2833.01	N/A	N/A	N/A	N/A		74.48

Table 4
Solar irradiance, ambient temperature and sunshine duration in Penryn.

Month	Global solar energy (kWh/m^2)	Diffuse solar energy (kWh/m^2)	Ratio of diffuse solar energy	Sunshine duration (h)	Effective clock time(h)		Effective sunshine duration (h)	S (W/m^2)	T_a (°C)	v_{wind} (w/s)	Mean incidence (°)	η_{opt}		Predicted electric energy (kWh/m^2)
					Start	Stop						Flat	CCPC	
Jan	44	21	0.477	248	8	17	279	177.42	7.3	8.06	55.33	0.962	0.129	3.68
Feb	63	29	0.460	280	7.5	17.5	280	225.00	6.9	7.22	52.17	0.969	0.138	4.83
Mar	106	52	0.491	372	7.6	18.5	337.9	284.95	7.8	6.94	48.42	0.975	0.150	7.65
Apr	146	67	0.459	420	7.2	18.5	339	347.62	9.2	5.83	47.38	0.976	0.153	9.50
May	164	79	0.482	465	7	19.5	387.5	352.69	11.8	5.83	44.12	0.980	0.168	11.37
Jun	164	79	0.484	480	6.8	19.5	381	341.67	14.4	5.00	44.28	0.980	0.167	10.80
Jul	149	84	0.564	496	6.9	19.8	399.9	300.40	15.8	4.72	45.12	0.979	0.163	9.84
Aug	145	78	0.538	434	7.2	19.8	390	334.10	16.2	4.44	46.10	0.978	0.159	10.62
Sep	126	55	0.437	360	7.2	19.5	369	350.00	14.7	5.56	50.19	0.972	0.144	10.18
Oct	87	41	0.471	341	7.4	18.5	344.1	255.13	12.4	6.94	53.24	0.966	0.135	6.70
Nov	54	25	0.463	270	7.5	16.5	270	200.00	9.7	6.94	53.74	0.966	0.133	4.08
Dec	44	18	0.409	248	8	16	248	177.42	7.6	8.06	54.50	0.964	0.131	3.29
Year	1292	628	0.486	4414	N/A		4015.4	3346.40	N/A	N/A	N/A	N/A		92.52

Table 5
Solar irradiance, ambient temperature and sunshine duration in Jaen.

Month	Global solar energy (kWh/m^2)	Diffuse solar energy (kWh/m^2)	Ratio of diffuse solar energy	Sunshine duration (h)	Effective clock time(h)		Effective sunshine duration (h)	S (W/m^2)	T_a (°C)	v_{wind} (w/s)	Mean incidence (°)	η_{opt}		Predicted electric energy (kWh/m^2)
					Start	Stop						Flat	CCPC	
Jan	152	33	0.217	310	8.3	18	300.7	490.32	6.3	1.39	43.88	0.981	0.170	12.43
Feb	136	43	0.316	308	8	18.2	285.6	441.56	8.7	1.67	41.84	0.983	0.182	10.86
Mar	179	61	0.341	372	7.5	18.2	331.7	481.18	11.7	2.22	40.83	0.984	0.190	13.97
Apr	193	67	0.347	390	7.5	18.2	321	494.87	13.9	2.50	47.13	0.977	0.154	12.97
May	199	76	0.382	434	7	18.1	344.1	458.53	18.3	2.50	47.09	0.977	0.155	12.85
Jun	213	65	0.305	450	6.5	18.1	348	473.33	24.4	2.50	50.42	0.972	0.143	13.08
Jul	236	44	0.186	434	7	18.1	350.3	543.78	26.4	2.50	48.72	0.974	0.149	15.39
Aug	233	51	0.219	403	7.5	18.3	334.8	578.16	25.8	2.22	44.25	0.980	0.168	16.32
Sep	196	55	0.281	360	8	18.1	303	544.44	21.3	1.94	39.43	0.986	0.201	14.81
Oct	168	55	0.327	341	8.5	18	294.5	492.67	16.4	1.67	40.10	0.985	0.195	12.85
Nov	161	35	0.217	300	8	18	300	536.67	10	1.39	44.50	0.980	0.166	13.51
Dec	140	35	0.350	279	8.5	17	263.5	501.79	7	1.39	41.07	0.984	0.188	11.55
Year	2206	621	0.282	4381	N/A		3777.2	6037.31	N/A	N/A	N/A	N/A		160.58

However, note that a CPV/T module can no longer work when an incidence is higher than 90° because in this case, the solar beam has been incident on the back of the module, even though it is sunshine. Thus, the effective clock times and effective sunshine duration are proposed in the paper and have to be decided. The effective clock times include CPV/T start-working time at which the incidence is just 90° in the morning and CPV/T stop-working time at which the incidence becomes 90° once again in the evening. Naturally, the effective sunshine duration is determined from the difference between the CPV/T stop-working time and the start-working time. These data are tabulated in Tables 3–5 together with the mean wind speed in each month for Glasgow, Penryn and Jaen.

Finally, the monthly water temperature at the first heat exchanger inlet is needed for monthly performance predictions. Based on the three observations mentioned above, the water

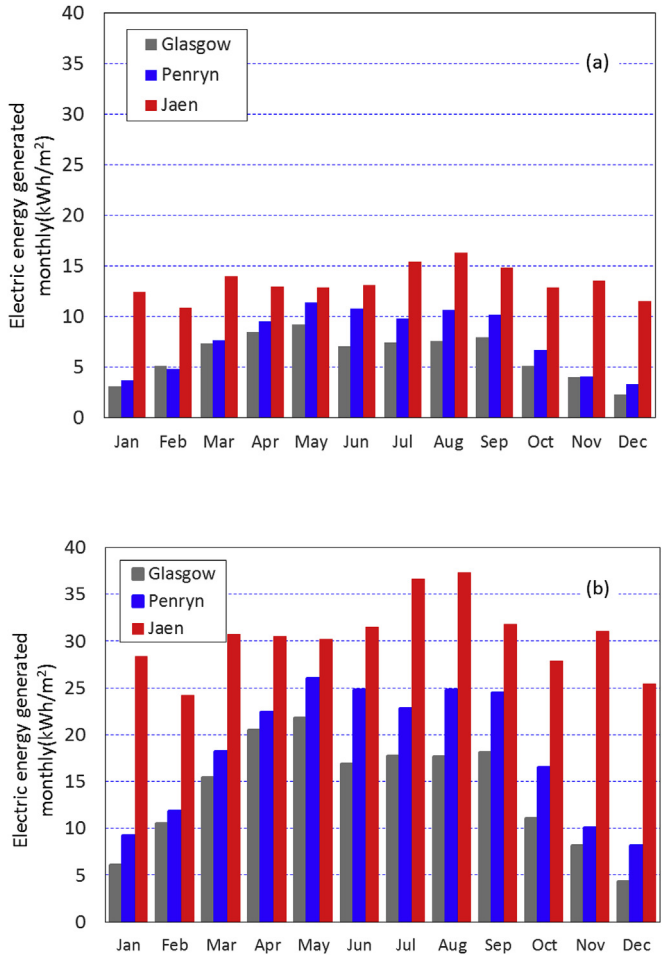

Fig. 12. Predicted monthly electric energy obtained with the CPV/T system in Glasgow, Penryn and Jaen, respectively, at (a) an off-optimal incidence shown in Tables 3–5, and (b) an optimal incidence.

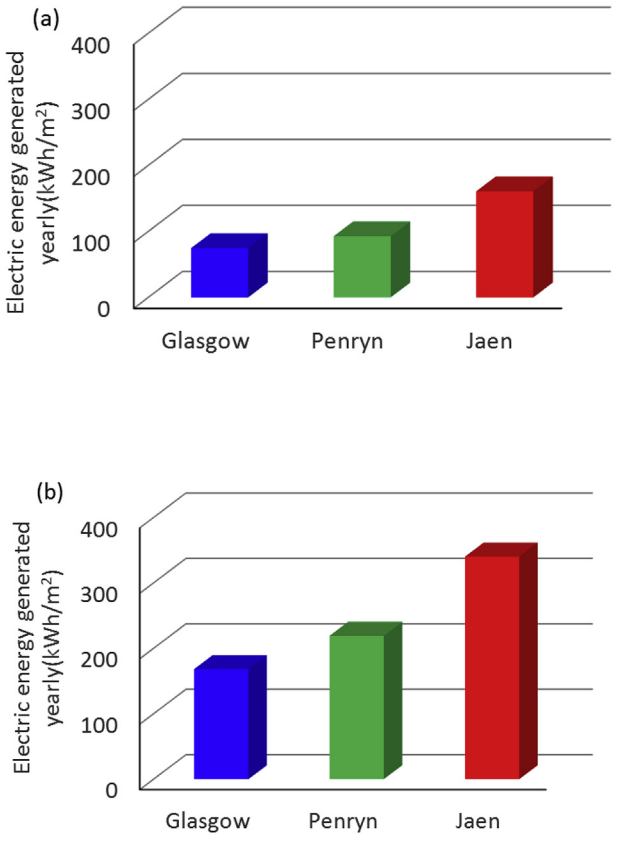

Fig. 13. Predicted annual electric energy obtained with the CPV/T system in Glasgow, Penryn and Jaen, respectively, at (a) an off-optimal incidence shown in Tables 3–5, and (b) an optimal incidence.

temperature can be correlated to the ambient temperature with the following expression,

$$T_{fij} = \left(2.3772 \times 10^{-2} j^2 - 3.4371 \times 10^{-1} j + 2.2997\right) T_a \qquad (9)$$

where j represents a month of year, $j = 1, 2, \ldots, 12$.

The synthetic climate data in Tables 3–5 are used as an input to the code with the water mass flow rate of 4.3 kg/min and Eq. (9), respectively. The predicted electric energy based on the maximum power points is illustrated in Tables 3–5 and for comparison the energy yield is illustrated in Fig. 12(a). As seen, in Glasgow and Penryn, the CPV/T system can perform well during March to September, compared to that in the other months. Further, the CPV/T system shows having a better electric performance in Penryn than that in Glasgow during April to October. And, overall, the CPV/T system performance in Penryn is better than in Glasgow. Particularly, in Jaen, the electric performance of the CPV/T system is the best all year-round in comparison with those in Glasgow and Penryn because its electric energy is doubled or more in January, February, March, October, November, and December.

Based on Tables 3–5, the mean incidences of solar beam against the glass cover in the CPV/T systems vary in a range of 33°-50° in Glasgow, 44° −55° in Penryn and 40°-51° in Jaen, and they are far away from the optimum range of 0°-20°. As a result, the CCPCs are subject to an optical efficiency as low as 14.2% in April in Glasgow, 12.9% in January in Penryn and 14.3% in June in Jaen, respectively, even though the flat PV models are with an optical efficiency of over 96%. This suggests that the flat PV/T modules are running nearly under the optimal condition but the PV/T modules with CCPC are operating under the off-optimal condition. To improve the CCPC optical performance further, a sun tracking device should be included with the PV/T system and the research on this is currently underway. If however the roof-top systems are operated within the optimal range of 0-20°, the model predicts that the corresponding monthly electric power could be approximately two times greater as shown in Fig. 12 (b), since in this case, the optical efficiency of the CCPCs is as high as 84% (Fig. 4).

Accordingly, the annual electric energy generated by the three systems is depicted in Fig. 13(a). The electric energy produced in Jaen is more than double compared to that in Glasgow, while the energy in Penryn is 20% higher than that in Glasgow. Similarly, if the solar radiation incidence on the three roof-top systems is maintained at the optimal incidence, the annual electricity yield from the systems, as illustrated in Fig. 13(b), is nearly 2.2 times that generated at the incidences outside the optimal range.

4.3. Discussion

4.3.1. Transient effect

In Section 3.4, the transient effect in Eq. (1) was neglected to simplify the model and solution procedure. To clarify its effect, the transient terms are switched on by providing the mass of the glass cover, PV cell, absorber, water and back cover per unit collecting area, such as $M_g = 7.5$ k g/m^2, $M_s = M_p = 8.5$ kg/m^2, $M_b = 5$ kg/m^2

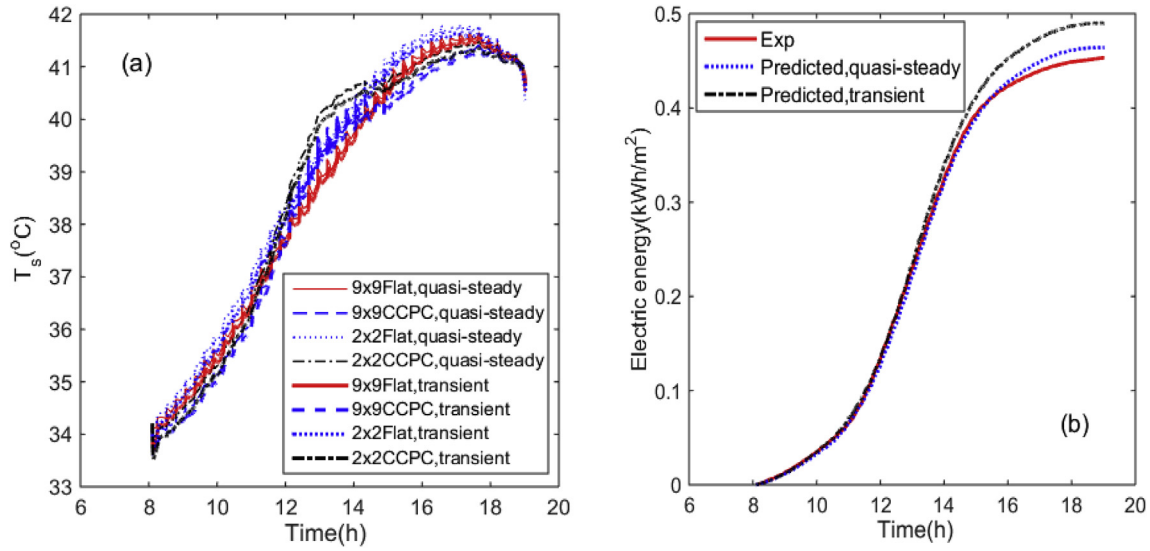

Fig. 14. Predicted cell temperature and electric energy obtained with CPV/T system on 11 July 2016 in Jaen based on transient model.

and $M_f = LA_h\rho_f/A_c$, where L, A_h and ρ_f are the length of flow channels in the heat exchanger, cross-sectional area of flow channels and water density, respectively.

Eq. (1) is a 1st-order ordinary differential equation system with variable heat transfer coefficients and can be solved by using a standard 2nd-order predictor-corrector Euler method, i.e. Heun method [42] with a time-step of 1.819 s to ensure the solution convergence. Moreover, since the heat transfer coefficients are dependent on unknown temperatures, the differential equations, Eq. (1), are integrated, and the heat transfer coefficients are updated in each time-step for ten cycles as described in Section 3.4.

To initiate the solution procedure, an initial temperature filed is set. Here the initial temperature of the top glass cover is assumed to be equal to the ambient temperature, while the initial values of the rest temperature are assigned to be the water temperature at the first heat exchanger inlet. In the observation, the sampling time for one I-V curve was 5.5 s, but the sampling time between two I-V curves was 461 s. These two sampling times are longer than the time-step required for simulation, therefore an interpolation scheme is employed to interpolate the observed data from the known coarse time profile to a profile with a fine time-step. Here a shape-preserving piecewise cubic interpolation of the values at neighbouring time grid points is chosen. Since the observed data in Jaen show less fluctuation, they are used in the transient simulation to reduce any potential errors in the interpolation.

Fig. 14 illustrates the cell temperature and electric energy obtained by the CPV/T system on 11 July 2016 in Jaen predicted by the transient model. The results from the quasi-steady model are plotted as well for making a comparison. It is clear that the cell temperature predicted from the transient model is lower than that from the quasi-steady model with a maximum difference of only 0.2 °C. Consequently, an over-predicted electric energy with an increased error of 8.07% against the experiment is resulted in comparison with the 2.38% error based on the quasi-steady model. Further, the transient terms in Eq. (1) defer the thermal response of heat exchangers, causing a slightly low cell temperature. This, in turn, shows the PV cells having an improved electrical performance. This further follows the fact that since the current of I-V curve is an exponential function of $1/T_s$, as shown in Eq. (7), any change in the cell temperature T_s leads to a considerable increased in the current and subsequently in the electric energy.

4.3.2. Diffuse radiation component

The diffuse solar radiation on the Earth is the solar beam which is reflected/scattered by suspended solid particle, water droplets and molecules in the atmosphere [26]. The diffuse radiation component is isotropic, when it reaches on the mirror or reflective film, and the radiation intensity of the reflected diffuse component is the same in all the direction. In other words, the diffuse radiation cannot be concentrated by a CCPC, and it is considered to be a beam with effective incidence angle onto the CCPC [43].

According to Tables 3–5, the ratio of the diffuse solar energy over the global solar energy depends on month, especially on the place where the CPV/T system is installed. For example, the mean ratios of diffuse solar energy are 0.488, 0.486 and 0.282 in Glasgow, Penryn and Jaen, respectively. To consider the diffuse radiation effect, the second and third equations in the heat transfer balance equations Eq. (1) are modified in the following manner while the rest remains unchanged,

$$\begin{cases} M_sC_s\dfrac{dT_s}{dt} = a_2S\times(1-d)\times CR\times\eta_{opt} + a_2S\times d\times 1/CR\times\eta_{opt1} - h_{sp}(T_s-T_p) - h_{sg}(T_s-T_g) - E_{PV} \\ M_pC_p\dfrac{dT_p}{dt} = a_3S\times(1-d)\times CR\times\eta_{opt} + a_3S\times d\times 1/CR\times\eta_{opt1} + h_{sp}(T_s-T_p) - h_{pg}(T_p-T_g) - h_{pb}(T_p-T_b) - h_{pf}\left(T_p-T_f\right) \end{cases} \quad (1b)$$

where d is the ratio of the diffuse irradiance over the global irradiance on a CPV/T module, η_{opt} is the optical efficiency of flat module or module with CCPC for the diffuse irradiance issued from

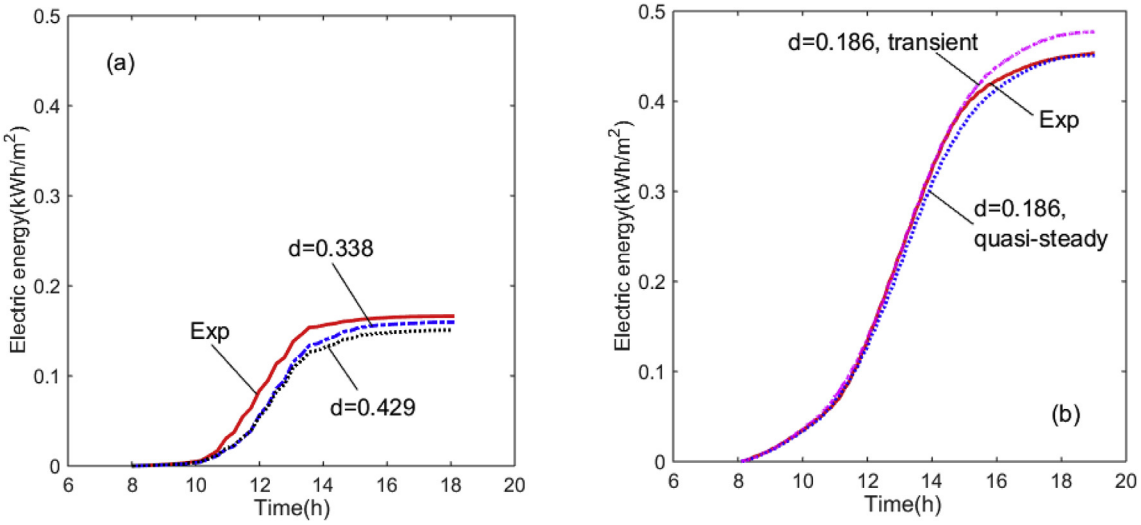

Fig. 15. Predicted electric energy curves by considering diffuse radiation component for the CPV/T systems on 19 March 2016 in Glasgow and on 11 July 2016 in Jaen, (a) Glasgow, based on quasi-steady model, (b) Jaen, based on quasi-steady and transient models.

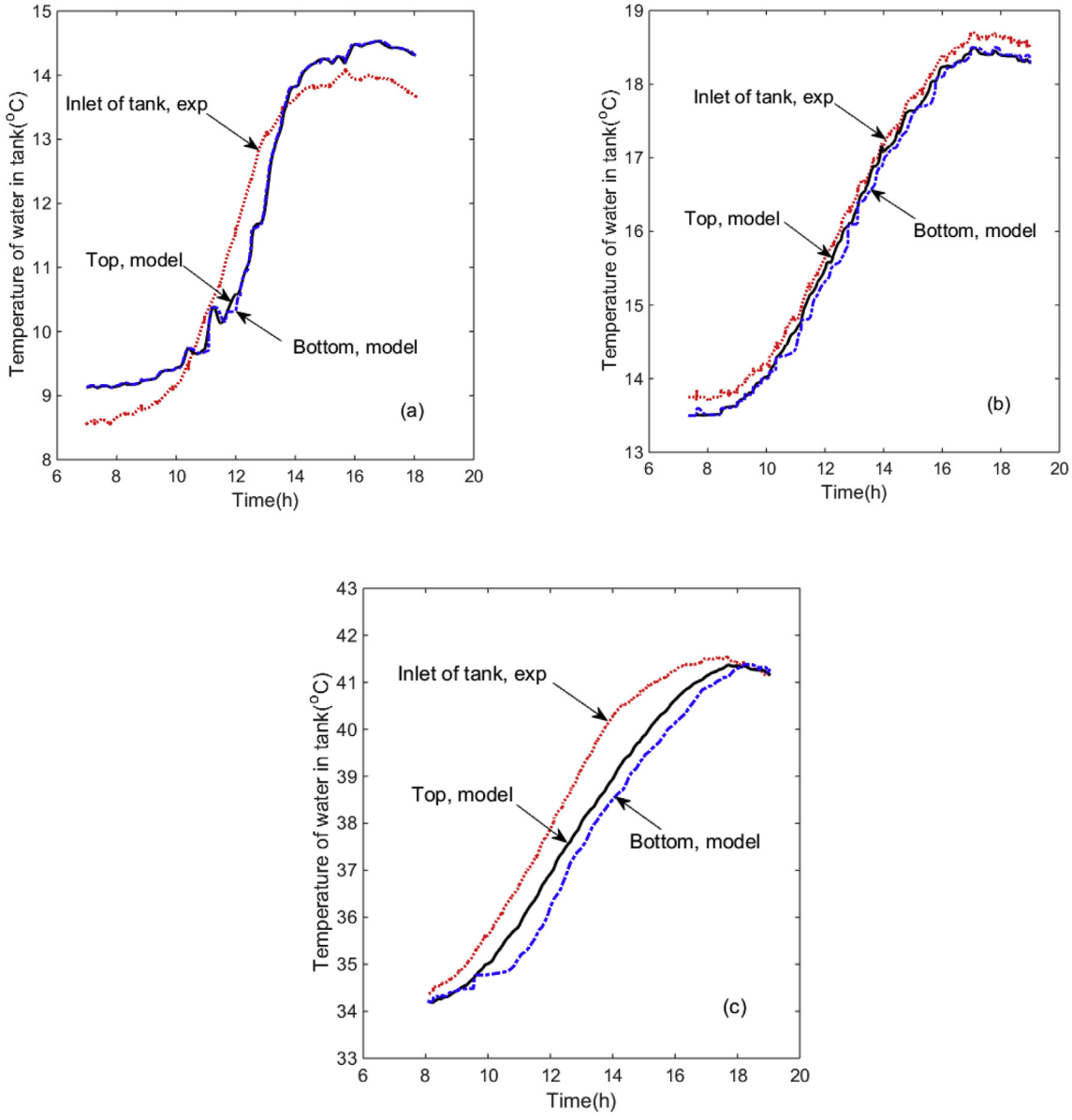

Fig. 16. A comparison of predicted temperature of water in the storage tank against the experimental data on 19 March 2016 in Glasgow, 11 July 2016 in Jaen, and 17 September 2015 in Penryn, (a) Glasgow, (b) Penryn, (c) Jaen, the water volume in the tank is 113.65 L.

the sky, and depends on the effective incidence angle determined with the following expression [43],

$$\theta_{eff} = 59.68 - 0.1388\beta + 0.001497\beta^2 \quad (10)$$

where β is the tilted angle of a CPV/T module. When the effective incidence is available, η_{opt1} can be estimated from Eq. (3). Accordingly, the irradiance for estimating the electric power via Eq. (6) is altered as $S \times (1-d) \times \eta_{opt} + S \times d \times \eta_{opt1}/CR$.

For the roof-top system in Glasgow, two cases are further investigated with the two ratios of the diffuse irradiance based on the quasi-steady model. From Table 3, the daily mean ratio of the diffuse irradiance in March is 0.429, thus, the first ratio of the diffuse irradiance is chosen to be $d = 0.429$. In Ref. [44], another daily mean ratio of the diffuse irradiance in March is given as 0.338, consequently, in the second case, $d = 0.338$. For the roof-top system in Jaen, the daily mean ratio of the diffuse irradiance is $d = 0.186$ in July based on Table 5. Hence this ratio is chosen in the quasi-steady and transient models, respectively.

The electrical energy profiles in these cases are illustrated in Fig. 15. For the roof-top system in Glasgow, the predictions with diffuse irradiance fall under the experimental data with $d = 0.338$ giving slightly better prediction, compared with Fig. 9(c). For the roof-top system in Jaen, since the ratio of diffuse irradiance is less than 0.2, its effect on the predictions is limited in both transient and quasi-steady models in comparison with Fig. 11(e). This thus suggests that if a ratio of the diffuse irradiance becomes less than 0.2, its effect can be negligible.

4.3.3. Thermal model for storage tank

Thermal modelling for storage tanks in solar energy application is a well-established subject; especially a multi-node/segment thermal model, proposed in Ref. [26], has been successfully applied in the thermal performance prediction of a stratified thermal storage tank [45], storage tanks for copolymer solar water collector [46], thermal solar collectors [47], and thermal collector in series [48,49]. In the model, the storage tank water body is divided into a number of equal volume segments from the water top surface to the bottom. In each segment the water temperature is constant, but it varies from one segment to another. The following heat transfer balance equation [46,47] is solved neglecting any heat loss from the connecting pipes and thermal load as well as heat conduction in the water body.

$$\rho_{fj} C_{fj} V_{fj} \frac{dT_j}{dt} = B^j \dot{m}_f C_{fj} \left(T_{fout} - T_j\right) + \dot{m}_{sj} C_{fj} (T_{j-1} - T_j) - h_t (T_j - T_a) \quad (11)$$

where ρ_{fj}, C_{fj} and V_{fj} are the water density, heat capacity and volume in the segment j^{th}, here $j = 1, 2, \ldots, N_t$, andN_t is the total number of segments, $N_t = 10$ [47]; T_j is the temperature of water in a tank; T_{fout} is the temperature of water at the outlet of the last heat exchanger of the CPV/T module, and it has been determined in the previous sections based on a known temperature of water at the inlet of the first heat exchanger; h_t is the heat transfer coefficient between the tank wall and the outside air, $h_t = 4.38$ W/K [50]. B^j is a control function, and $\dot{m}_{sj}$ is the mass flow rate between two segments, they are determined by the following equations [49]

$$B^j = \begin{cases} 1 & T_j \in \left[T_{fout}, T_{j-1}\right) \\ 0 & \text{otherwise} \end{cases} \text{ and } \dot{m}_{sj} = \dot{m}_f \sum_{l=1}^{j} B^l \quad (12)$$

Eq. (11) is incorporated into the thermal-optical-electrical modelling code and solved with the same numerical method presented in Section 4.3.1 at every 0.5 s time-step to predict the temperature of water with 113.65 L volume in the storage tank on 19 March 2016 in Glasgow, 11 July 2016 in Jaen, and 17 September 2015 in Penryn, respectively. As seen in Fig. 16, the temperature of water in the top segment is nearly the same as the temperature of water in the bottom segment. It thus suggests that the water is well mixed and does not exhibit any stratified effect. A comparison is also made against the experimental water temperature profile at the inlet of the tank and shown in Fig. 16. While the Penryn data seem to give excellent agreement, the model underpredicts the water temperature in the Jaen system. In Glasgow, a variation is also seen, but generally a less than 2 °C difference is found in the Glasgow and Jaen modules when comparing between the predicted and observation data.

5. Conclusion

In the article, a coupled lumped optical, thermal and electrical model is developed for roof-top PV/T systems with and without CCPC and applied to predict the electrical performance of such systems installed in Glasgow, Penryn and Jaen. It is demonstrated that the proposed model is reasonable and feasible in predicting the electrical performance of the systems with a mean error in the range of 2–14% for electrical energy. Long-term as well as monthly electric performance of the systems in the three places is also predicted based on the synthetic climate data generated with Meteonorm 7. The system demonstrates better performance in Jaen than in either Glasgow or Penryn. This is due to higher direct normal irradiance under the Jaen climate conditions. Transient terms and diffuse irradiance are significant on influencing the electric energy profile, however, the diffuse irradiance effect can be ignored if the ratio of diffuse irradiance over the global irradiance is less than 0.2. It is identified that all the systems are subject to an incidence larger than 10°, causing the CPV/T systems to exhibit unsatisfactory performance. Further work should include outdoor observation of diffuse irradiance as well as development of a sun tracking device.

Acknowledgment

The authors gratefully acknowledge financial support received from the EPSRC through SUPERGEN Solar Challenge Project SUNTRAP (EP/K022156/1).

Appendix. Empirical formulas for natural and forced heat transfer coefficients

Based on experimental data for natural convection heat transfer in parallel plates, which resemble to the case in flat PV/T module with filled air between the top glass cover and the PV cells, the following correlation was proposed to estimate the Nusselt number [36]

$$\mathrm{Nu} = 1 + 1.44\left[1 - \frac{1708(\sin 1.8\,\beta)^{1.6}}{\mathrm{Racos}\,\beta}\right]\left[1 - \frac{1708}{\mathrm{Racos}\,\beta}\right]^{+} + \left[\left(\frac{\mathrm{Racos}\,\beta}{5830}\right)^{1/3} - 1\right]^{+} \quad (A1)$$

where the meaning of the + exponent is that if the values of the terms in the [ ] are positive, then they are used, otherwise, the values are zero; the Nusselt number is related to natural convection heat transfer coefficient, h_{con}, namely, $\mathrm{Nu} = h_{con} b/k$, b is the gap between two plates, k is air thermal conductivity, W/(m K), β is

inclination angle of two plates, Ra is Rayleigh number of the air between the plates, $Ra = g\beta'(T_{hot} - T_{cold})b^3/\nu\tau$, g is gravitational constant, β' is volumetric coefficient of expansion of air, T_{hot} and T_{cold} are the highest and lowest temperature of two plates, K, ν is kinematic viscosity, m^2/s, τ is thermal diffusivity of air, m^2/s.

For natural convection heat transfer in a CPC cavity, a series of experiments were conducted in Ref. [37] on variable *CR* and inclination angle, the average Nusselt number on the top glass cover was correlated to Rayleigh number by the following relation

$$Nu = c_1[\cos(\beta - c_2)]^{n_1} Ra^{n_2} \tag{A2}$$

where values for the parameters are given in Table A1. The correlation is applicable for values of $Nu > 1$, $30^\circ < \beta < 90^\circ$ and $Ra < 10^7$ for $CR = 2, 3$ and $Ra < 10^6$ for $CR = 4, 5$[37]; Definitions of Nusselt number and Rayleigh number are as the same above.

An analytical forced convection heat transfer coefficient was proposed in Ref. [40] for plate fin heat sinks and the fin efficiency has been considered. The average Nusselt number over the fins is calculated by the following expression

$$Nu_b = \frac{\tanh\sqrt{2Nu_i \frac{k}{k_{fin}} \frac{H}{b} \frac{H}{\delta}\left(\frac{\delta}{L}+1\right)}}{\sqrt{2Nu_i \frac{k}{k_{fin}} \frac{H}{b} \frac{H}{\delta}\left(\frac{\delta}{L}+1\right)}} Nu_i \tag{A3}$$

The Nusselt number in fin channels is expressed as

$$Nu_i = \left[\frac{1}{\left(Re_b^* Pr/2\right)^3} + \frac{1}{\left(0.664\sqrt{Re_b^*}\, Pr^{1/3}\sqrt{1+\frac{3.65}{\sqrt{Re_b^*}}}\right)^3}\right]^{-1/3} \tag{A4}$$

where $Re_b^* = Re_b(b/L)$, $Re_b = Ub/\nu$, U is mean fluid velocity in fin channels, b is fin channel spacing, L is fin length, H is fin height, δ is thickness of fin, k is fluid thermal conductivity, k_{fin} is fin thermal conductivity, Pr is fluid Prandtl number, $Pr = \nu/\tau$, the Nusselt number of fins is defined as $Nu_b = h_{fin}b/k$, h_{fin} will be either h_{pf} or h_{bf} in Eq. (1) or (1a).

Table A1
Values of correlation parameters in Eq. (A2).

CR	c_1	c_2(deg)	n_1	n_2
2	0.201	48	1/3	0.238
3	0.145	63	1/3	0.25
4	0.0468	63	1/2	0.325
5	0.0168	65	1/2	0.39

References

[1] Kern E C and Russell M C, 1978, Combined Photovoltaic and thermal hybrid collector systems, Proceedings of 13th IEEE Photovoltaic Specialists' Conference, Washington DC, 5–8 June, USA.
[2] A. Suzuki, S. Kitamura, Combined photovoltaic and thermal hybrid collector, Jpn. J. Appl. Phys. Suppl. 19 (2) (1980) 79–83.
[3] S.B. Riffat, E. Cuce, A review on hybrid phototoxic/thermal collectors and systems, Int. J. Low-Carbon Technol. 6 (2011) 212–241.
[4] V.V. Tyagi, S.C. Kaushik, S.K. Tyagi, Advancement in solar photovoltaic/thermal (PV/T) hybrid collector technology, Renew. Sustain. Energy Rev. 16 (2012) 1383–1398.
[5] B.J. Huang, T.H. Lin, W.C. Hung, F.S. Sun, Performance evaluation of solar photovoltaic/thermal systems, Sol. Energy 70 (5) (2001) 443–448.
[6] S.A. Kalogirou, Use of TRNSYS for modelling and simulation of a hybrid pv-thermal solar system for Cyprus, Renew. Energy 23 (2001) 247–260.
[7] S.A. Kalogirou, Y. Tripanagnostopoulos, Hybrid PV/T solar systems for domestic hot water and electricity production, Energy Convers. Manag. 47 (18–19) (2006) 3368–3382.
[8] Y. Tripanagnostopoulos, Aspects and improvements of hybrid photovoltaic/thermal solar energy systems, Sol. Energy 81 (9) (2007) 1117–1131.
[9] J. Ji, J. Han, T.T. Chow, H. Yi, J. Lu, W. He, W. Sun, Effect of fluid flow and packing factor on energy performance of a wall-mounted hybrid photovoltaic/water-heating collector system, Energy Build. 38 (2006) 1380–1387.
[10] T.T. Chow, Energy and exergy analysis of photovoltaic-thermal collector with and without glass cover, Appl. Energy 86 (2009) 310–316.
[11] M. Herrando, C.N. Markides, K. Hellgardt, A UK-based assessment of hybrid PV and solar-thermal systems for domestic heating and power: system performance, Appl. Energy 122 (2014) 288–309.
[12] I. Guarracino, A. Mellor, N.J. Ekins-Daukes, C.N. Markides, Dynamic coupled thermal-and-electrical modelling of sheet-and-tube hybrid photovoltaic/thermal (PVT) collectors, Appl. Therm. Eng. 101 (2016) 778–795.
[13] N. Sellami, T.K. Mallick, Optical efficiency study of PV crossed compound parabolic concentrator, Appl. Energy 102 (2013) 868–876.
[14] W. Li, C.M. Paul, N. Sellami, et al., Coupled simulation of performance of a crossed compound parabolic concentrator with solar cell, Energy Procedia 75 (2015) 325–330.
[15] C.K. Hsieh, Thermal analysis of CPC collectors, Sol. Energy 27 (1981) 19–29.
[16] R. Tchida, N. Ngos, A Theoretical evaluation of the thermal performance of CPC with flat one-sided absorber, Int. Commun. Heat Mass Transf. 33 (2006) 709–718.
[17] R. Tchida, Thermal behaviour of solar air heater with compound parabolic concentrator, Energy Convers. Manag. 49 (2008) 529–540.
[18] D.K. Patel, P.K. Brajmbhatt, Analysis and performance investigations on a solar air heater with compound parabolic concentrator, Int. J. Recent Innovation Trends Comput. Commun. 3 (2) (2015) 64–71.
[19] H.P. Garg, R.S. Adhikari, Performance analysis of a hybrid photovoltaic/thermal (PV/T) collectors with integrated CPC troughs, Int. J. Energy Res. 23 (1999) 1295–1304.
[20] M.Y.H. Othman, B. Yatim, K. Sopian, M.N. Abu Bakar, Performance analysis of a double-pass photovoltaic/thermal (PV/T) solar collector with CPC and fins, Renew. Energy 30 (2005) 2005–2017.
[21] J. Sun, M.H. Shi, Numerical study on optical and electric-thermal performance for solar concentrating PV/T air system, Sci. China Ser. E Technol. Sci. 52 (12) (2009) 3514–3520.
[22] Maifi L, Chari A, Hioual O and Kerbache T, 2013, Study and modelling of a photovoltaic thermal hybrid solar collector with cylindro-parabolic concentrator, Proceedings of International Conference on Renewable Energy Resources, Tunisia.
[23] G.Q. Li, G. Pei, Y.H. Su, X. Zhou, J. Ji, Preliminary study based on building-integrated compound parabolic concentrators (CPC) PV/thermal technology, Energy Procedia 14 (2012) 343–350.
[24] H.M. Bahaidarah, B. Tanweer, P. Gandhidasan, S. Rehman, A combined optical, thermal and electrical performance study of a V-trough PV system-Experimental and analytical investigation, Energies 8 (2015) 2803–2827.
[25] T. Kostic Lj, T.M. Pavlovic, Z.T. Pavolvic, Optimal design of orientation of PV/T collector with reflectors, Appl. Energy 87 (2010) 3023–3029.
[26] J.A. Duffie, W.A. Beckman, Solar Engineering of Thermal Processes, fourth ed., Hoboken: John & Sons, Inc., USA, New Jersey, 2013.
[27] M.U. Siddiqui, A.F.M. Arif, L. Kelly, S. Dubowsky, Three-dimensional thermal modelling of a photovoltaic module under varying condition, Sol. Energy 86 (2012) 2620–2631.
[28] A.P. Dobos, An improved coefficient calculator for the California Energy Commission 6 parameter photovoltaic model, ASME J. Sol. Energy Eng. 134 (2012), 021011-1-6.
[29] W. De Soto, S.A. Klein, W.A. Beckman, Improvement and validation of a model for photovoltaic array performance, Sol. Energy 80 (2006) 78–88.
[30] H.P. Garg, R.S. Adhikari, Transient simulation of conventional hybrid photovoltaic/thermal (PV/T) air collectors, Int. J. Energy Res. 22 (1998) 547–562.
[31] W. Li, M.C. Paul, N. Sellami, et al., Six-parameter electrical model for photovoltaic cell/module with crossed compound parabolic concentrator, Sol. Energy 137 (2016) 551–563.
[32] W. Li, M.C. Paul, et al., A Scaling Law for Monocrystalline for Photovoltaic/thermal Modules with Crossed Compound Parabolic Concentrators, 2016 (submitted for publication).
[33] W. Li, M.C. Paul, et al., Thermal performance of two heat exchangers for thermoelectric generators, Case Stud. Therm. Eng. 6 (2016) 164–175.
[34] A.A. Sfeir, Monthly average optical efficiency of flat plate collectors, Sol. Energy 30 (1983) 397–399.
[35] E.A. Sjerps-Koomen, E.A. Alsema, W.C. Turkenburg, A simple model for PV module reflection losses under field Conditions, Sol. Energy 57 (1996) 421–432.
[36] K.G.T. Hollands, T.E. Unny, G.D. Raithby, L. Konicek, Free convection heat transfer across inclined air layers, ASME J. Heat Transf. 98 (1976) 189–193.
[37] B.A. Meyer, J.W. Mitchell, M.M. El-Wakil, Convective heat transfer in vee-trough linear concentrators, Sol. Energy 28 (1) (1982) 33–40.
[38] D.T. Lobera, S. Valkealahti, Dynamic thermal model of solar PV systems under varying climate conditions, Sol. Energy 93 (2013) 183–194.
[39] K.S. Ong, Thermal performance of solar air heaters: mathematical model and

solution procedure, Sol. Energy 55 (2) (1995) 93–109.
[40] Teertstra P, Yovanovich M M and Culham J R, 1999, Analytical forced convection modelling of plate fin heat sinks, 15th IEEE SEMI-THERMTM Symposium, p.34–41.
[41] E.F. Fernández, F. Almonacid, P. Rodrigo, P. Pérez-Higueras, Calculation of the cell temperature of a high concentrator photovoltaic (HCPV) module: a study and comparison of different methods, Sol. Energy Mater. Sol. Cells 121 (2014) 144–151.
[42] S.C. Chapra, R.P. Canale, Numerical Methods for Engineers, sixth ed., The McGraw-Hill Companies, Boston, 2010, pp. 719–724.
[43] E. Strobach, D. Faiman, S.J. Bader, S.J. Hile, Effective incidence angles of sky-diffuse and ground-reflected irradiance for various incidence angle modifier types, Sol. Energy 89 (2013) 81–88.
[44] H. Ayoub, Improving the Energy Capture of Solar Collectors, MSc Thesis, University of Strathclyde, 2012, pp. 32–33.
[45] E.M. Kleinbach, W.A. Beckman, S.A. Klein, Performance study of one-dimensional models for stratified thermal storage tanks, Sol. Energy 50 (2) (1993) 155–166.
[46] C. Cristofari, G. Notton, P. Poggi, A. Louche, Modelling and performance of a copolymer solar water heating collector, Sol. Energy 72 (2) (2002) 99–112.
[47] C. Cristofari, G. Notton, P. Poggi, A. Louche, Influence of the flow rate and tank stratification degree of the performances of a solar flat-plate collector, Int. J. Therm. Sci. 42 (2003) 455–469.
[48] Y.D. Kim, K. Thu, H.K. Bhatia, C.S. Bhatia, K.C. Ng, Thermal analysis and performance optimization of a solar hot water plant with economic evaluation, Sol. Energy 86 (2012) 1378–1395.
[49] K. Zelzouli, A. Guizani, R. Sebai, C. Kerkeni, Solar thermal systems performances versus flat plate solar collectors connected in series, Engineering 4 (2012) 881–893.
[50] S. Dubey, G.N. Tiwari, Thermal modelling of a combined system of photovoltaic thermal (PV/T) solar water heater, Sol. Energy 82 (2008) 602–612.